

Influence of atmospheric deposition on biogeochemical cycles in an oligotrophic ocean system

France Van Wambeke¹, Vincent Taillandier², Karine Desboeufs³, Elvira Pulido-Villena¹, Julie Dinasquet^{4,5}, Anja Engel⁶, Emilio Marañón⁷, Céline Ridame⁸, Cécile Guieu²

5

¹ Aix-Marseille Université, CNRS/INSU, Université de Toulon, IRD, Mediterranean Institute of Oceanography (MIO) UM 110, 13288, Marseille, France

² CNRS, Sorbonne Université, Laboratoire d'Océanographie de Villefranche (LOV), UMR7093, 06230 Villefranche-sur-Mer, France

10 ³ LISA, UMR CNRS 7583, Université Paris-Est-Créteil, Université de Paris, Institut Pierre Simon Laplace (IPSL), Créteil, France

⁴ Sorbonne Universités, Laboratoire d'Océanographie Microbienne (LOMIC), Observatoire Océanologique, 66650, Banyuls/mer, France

⁵ Marine Biology Research Division, Scripps Institution of Oceanography, UCSD, La Jolla, USA

15 ⁶ GEOMAR – Helmholtz-Centre for Ocean Research, Kiel, Germany

⁷ Department of Ecology and Animal Biology, Universidade de Vigo, 36310 Vigo, Spain

⁸ Sorbonne University/CNRS/IRD/MNHN, LOCEAN: Laboratoire d'Océanographie et du Climat: Expérimentation et Approches Numériques, UMR 7159, 4 Place Jussieu – 75252 Paris Cedex 05, France

20 *Correspondence to:* France Van Wambeke (france.van-wambeke@mio.osupytheas.fr) and Cécile Guieu (guieu@imev-mer.fr)

Abstract.

The surface mixed layer (ML) in the Mediterranean Sea is a well stratified domain characterized by low macro-nutrients and low chlorophyll content, for almost 6 months of the year. In this study we characterize the biogeochemical cycling of nitrogen (N) in the ML by analysing simultaneous *in situ* measurements of atmospheric deposition, nutrients in seawater, hydrological conditions, primary production, heterotrophic prokaryotic production, N₂ fixation and leucine aminopeptidase activity. Dry deposition was continuously measured across the central and western open Mediterranean Sea and two wet deposition events were sampled, one in the Ionian Sea and one in the Algerian Basin. Along the transect, N budgets were computed to compare the sources and sinks of N in the mixed layer. *In situ* leucine aminopeptidase activity made up 14 to 66 % of the heterotrophic prokaryotic N demand, and the N₂ fixation rate represented 1 to 4.5 % of the phytoplankton N demand. Dry atmospheric

deposition of inorganic nitrogen, estimated from dry deposition of (nitrate and ammonium) in aerosols, was higher than the N₂ fixation rates in the ML (on average 4.8-fold). The dry
35 atmospheric input of inorganic N represented a highly variable proportion of biological N demand in the ML among the stations, 10 - 82% for heterotrophic prokaryotes and 1-30% for phytoplankton. As some sites were visited during several days the evolution of biogeochemical properties in the ML and within the nutrient-depleted layers could be followed. At the Algerian Basin site, the biogeochemical consequences of a wet dust
40 deposition event were monitored through high frequency sampling of CTD casts. Notably, just after the rain, nitrate was higher in the ML than in the nutrient depleted layer below. Estimates of nutrient transfer from the ML into the nutrient depleted layer could explain up to a third of the nitrate loss from the ML. Phytoplankton did not benefit directly from the atmospheric inputs into the ML, probably due to high competition with heterotrophic
45 prokaryotes, also limited by N and phosphorus (P) availability at the time of this study. Primary producers decreased their production after the rain, but recovered their initial state of activity after a 2-day lag in the vicinity of the deep chlorophyll maximum layer.

1. Introduction

50 The Mediterranean Sea (MS) is a semi-enclosed basin characterized by active ventilation and short residence times of the newly formed waters, due to its own thermohaline circulation (Mermex Group, 2011). In terms of biogeochemistry, the MS is characterized by a long summer stratification period, a west-to-east gradient of increasing oligotrophy, and a deficit in phosphorus (P) compared to nitrogen (Mermex Group, 2011). The last feature is confirmed by
55 a deep N/P ratio for inorganic nutrients, higher than the Redfield ratio, that increases toward the east (Krom et al., 2004).

The relationship between photoautotrophic unicellular organisms and heterotrophic prokaryotes (competition or commensalism) is affected by the balance of light and nutrients as well as possible inputs of organic matter from river runoff or atmospheric deposition.

60 Phytoplankton generally experience P, or N limitation, or both (Thingstad et al., 2005 ; Tanaka et al., 2011, Richon et al., 2018), whereas heterotrophic prokaryotes are usually P limited, or P and organic carbon co-limited (Sala et al., 2002, Van Wambeke et al., 2002, C ea et al., 2014).

The MS continuously receives anthropogenic aerosols, originating from industrial and
65 domestic activities around the basin and from other parts of Europe, along with pulsed natural

inputs from the Sahara. It is thus a natural LNLC study area, well adapted to investigate the role of ocean–atmosphere exchanges of particles and gases on marine biogeochemical cycles. Recent studies describe annual records of atmospheric deposition of trace metals and inorganic macronutrients (N, P) obtained at several locations around the MS (Markaki et al., 2010; Guieu and Ridame, in press; Desboeufs, in press). All records show pulsed and highly variable atmospheric inputs. Recent models and observations show that atmospheric deposition of organic matter (OM) is also highly variable and that their annual inputs are of the same order of magnitude as river inputs (Djaoudi et al., 2017, Kanakidou et al., 2018; Kanakidou et al., 2020; Galetti et al., 2020). Moreover, the sum of atmospheric inputs of nitrate, ammonium and soluble organic nitrogen has been shown to be equivalent or higher than those from N₂ fixation (Sandroni et al., 2007). In addition inorganic atmospheric N inputs alone may also be higher than N₂ fixation rates (Bonnet et al., 2011).

Aerosol amendments in bottles, minicosms or mesocosms have been widely used to study trophic transfer and potential export, as they allow natural communities to be studied under controlled conditions (i.e. Guieu et al., 2010; Herut et al., 2016; Mescioglou et al., 2019). Both diversity and functioning of various biological compartments are impacted by aerosol additions in different waters tested in the MS (Guieu and Ridame, in press, and Figure 3 therein). Differences in the biological responses have been observed, depending on the mode of deposition simulated (wet or dry), the type of aerosols used (natural or anthropogenic) and the *in situ* biogeochemical conditions at the time of the experiment (Guieu and Ridame, in press).

A fraction of organic carbon from aerosols is soluble, and this soluble fraction is partly available to marine heterotrophic prokaryotes (Djaoudi et al., 2020). Heterotrophic prokaryotes have the metabolic capacity to respond quickly to aerosol deposition through growth and changes in community composition (Rahav et al., 2016; Pulido-Villena et al., 2008; 2014), while the phytoplankton community responds more slowly or not at all (Guieu and Ridame, in press, and reference therein).

Owing to the intrinsic limitations of experiments in enclosures, which vary depending on the volume and design (i.e. the omission of higher trophic levels, absence of turbulent mixing limiting exchanges by diffusion, and wall effects) such experiments cannot fully simulate *in situ* conditions (Guieu and Ridame, in press). Thus, *in situ* observations are required to understand the consequences of aerosol deposition on biogeochemical cycling in the world's ocean. Such *in situ* studies are scarce and require dedicated, high-frequency sampling to

100 follow the effects of deposition on the biogeochemical processes while taking into account the water column dynamics as recently emphasized in cases studies (Pulido-Villena et al., 2008 and Rahav et al., 2016).

Hence, there is a need for sampling surveys with adaptive strategies to follow aerosol deposition events *in situ* and their impacts on biogeochemical processes, especially in the open waters of the stratified and nutrient limited MS. The objectives of the PEACETIME project were to study fundamental processes and their interactions at the ocean–atmosphere interface following atmospheric deposition (especially of Saharan dust) in the Mediterranean Sea, and how these processes impact the functioning of the pelagic ecosystem (Guieu et al., 2020).

110 As atmospheric deposition affects primarily the surface mixed layer (ML), the present study focuses on the upper part of the nutrient depleted layer that extends down to the nutriclines (as defined by Du et al., 2017). During the stratification period, concentrations of nitrate and phosphate inside the ML are often below the detection limits of standard methods. However, nanomolar concentrations of nitrate (and phosphate) can now be assessed accurately through the Long Waveguide Capillary Cell (LWCC) technique (Zhang and Chi, 2002), which permits the measurement of fine gradients inside nutrient depleted layers of the MS (Djaoudi et al., 2018).

The aims of the present study were to assess the impact of atmospheric nutrient deposition on biogeochemical processes and fluxes in the open sea during the PEACTIME cruise in the MS. For this i) we estimated nanomolar variations of nitrate concentration in the surface mixed layer (ML) under variable inputs of dry and wet aerosol deposition and ii) we compared the aerosol-derived N inputs to the ML with biological activities: primary production, heterotrophic prokaryotic production, N₂ fixation and ectoenzymatic (leucine aminopeptidase) activity. We studied the N budgets along a zonal transect that includes 13 stations crossing the Algerian Basin, Tyrrhenian Sea and the Ionian Sea where dry atmospheric deposition was continuously measured on board together with seawater biogeochemical, biological and physical characteristics. We finally focused on a wet deposition event that occurred in the western Algerian Basin, where we investigated the evolution of biogeochemical fluxes of both N and P and microbial activities through high frequency sampling.

130 **2. Materials and Methods**

2.1 Sampling strategy and measured parameters

The PEACETIME cruise (doi.org/10.17600/15000900) was conducted in the Mediterranean Sea, from May to June 2017, along a transect extending from the Western Basin to the center of the Ionian Sea (Fig. 1). For details on the cruise strategy, see Guieu et al. (2020). Short duration stations (< 8 h, 10 stations named ST1 to ST10, Fig. 1) and long duration sites (5 days, 3 sites named TYR, ION and FAST) were occupied. Chemical composition of aerosols was quantified by continuous sampling along the whole transect. In addition, two rain events were sampled (Desboeufs et al., 2021.), one on the 29th of May at ION, and a second one, a dust wet deposition event, at FAST on the 5th of June.

At least 3 CTD casts were conducted at each short station. One cast focused on the epipelagic layer (0-250 m), another on the whole water column. Two casts were carried out with a standard, CTD rosette equipped with 24 Niskin bottles (12 L), and a Sea-Bird SBE9 underwater unit with pressure, temperature (SBE3), conductivity (SBE4), chlorophyll fluorescence (Chelsea Acquatracka) and oxygen (SBE43) sensors. A third cast, from the surface to the bottom of the water column was carried out under trace metal clean conditions using an instrumental package including a titanium rosette (hereafter TMC-rosette) mounted on a Kevlar cable and equipped with Go-Flo bottles that were sampled in a dedicated clean lab container. The long duration sites were abbreviated as TYR (situated in the center of the Tyrrhenian Basin), ION (in the center of the Ionian Basin) and FAST (in the western Algerian Basin). These 3 sites were selected based on satellite imagery, altimetry and Lagrangian diagnostics as well as forecasted rain events (Guieu et al., 2020). At these sites, repeated casts were performed over at least 4 days with alternating CTD- and TMC- rosettes (Table 1). The succession of CTD casts at the FAST site is numbered in days relative to a rain event sampled on board the ship. The first cast of the series was sampled 2.3 days before the rain event, and the last 2 days after. The FAST site was revisited following the study at ST10 (3.8 days after the rain event).

Primary production (PP), prokaryotic heterotrophic production (BP), heterotrophic prokaryotic abundances (hprok), ectoenzymatic activities (leucine aminopeptidase (LAP) and alkaline phosphatase (AP)), were determined on water samples collected with the standard CTD-rosette. Dissolved inorganic nutrients, dissolved organic nitrogen (DON) and phosphorus (DOP) were measured on water samples collected using the TMC-rosette. LAP and AP were determined from two layers in the epipelagic waters (5 m depth and deep chlorophyll maximum (DCM)) at the short stations and at the ION and TYR sites. In addition,

LAP and AP were determined at 4 depths between 0 and 20 m for 4 profiles at FAST site, to
165 determine the variability within the ML.

2.2 Analytical methods and fluxes calculations

2.2.1 Nutrients in the atmosphere

Total suspended aerosol particles (TSP inlet) were collected continuously throughout the
170 campaign for dry deposition estimations. Aerosol sampling was carried out using filtration
units on adapted membranes for off-line chemical analysis (Tovar-Sanchez et al., 2020).
Simultaneously, water soluble fraction of the aerosols was sampled continuously, using a
Particle-into-Liquid-Sampler (PILS, Orsini et al., 2003). Moreover, two wet deposition events
were sampled, one at ION, one at FAST using rain collectors with on-line filtration (porosity
175 0.2 μm) (details in Desboeufs et al., 2021).

Nitrate and ammonium concentrations in the aerosols, abbreviated in the text as NO_3 and
 NH_4 respectively, were analyzed continuously on board from May 13th, using PILS sampling
coupled on-line with double way ion chromatography (PILS-IC, Metrohm, model 850
Professional IC with Metrosep A Supp 7 column for anion measurements and Metrosep C4
180 column for cation measurements). The temporal resolution for PILS-IC analysis was 70 min
for anions and 32 min for cations. Dissolved Inorganic Nitrogen (DIN) fluxes released by dry
deposition were estimated by multiplying NO_3 and NH_4 obtained through PILS-CI
measurements (nitrite concentrations were under analytical detection limits) by the dry
settling velocities of N-bearing aerosols, i.e 0.21 and 1 cm s^{-1} for NH_4 and NO_3 , respectively
185 (Kouvarakis et al., 2001). Mean NO_3 and NH_4 concentrations were calculated from the PILS-
IC data measured (1) during the occupation of each short station lasting between 0.13 and
0.66 days (with on average 5 measurements for NO_3 and 11 measurements for NH_4), and (2)
between two successive casts at the sites with a time lag between 0.4 and 1.21 days (with on
average 15 measurements for NO_3 and about 30 for NH_4). At ST1, NH_4 and NO_3
190 concentrations were obtained using IC analyses following water extraction from aerosol filter
sampling as the PILS-IC was not operational.

Total dissolved phosphate (TDP) concentrations were estimated from soluble P
concentrations extracted from particulate aerosols collected on filters after ultrapure water
extraction HR-ICP-MS analysis (Neptune Plus, Thermo Scientific TM) (Fu et al., this issue, in
195 prep) since it was generally below the detection limits of the PILS-IC technique. The
frequency of TDP analysis was therefore less than for NO_3 and NH_4 (0.28 -1.15 days

depending on the stations). At ION, TYR and FAST, filters collected aerosols at different periods including each one CTD cast, when possible.

200 Atmospheric deposition of soluble P was estimated by multiplying the TDP concentration by a dry settling velocity of 1 cm s^{-1} , except at FAST where 3 cm s^{-1} was used as this value is better adapted for lithogenic particles (Izquierdo et al., 2012). The dissolved fraction and solution from digestion (Heimburger et al., 2012) of particulate fractions in the filters were analysed by ICP-AES (Inductively Coupled Plasma Atomic Emission Spectrometry, Spectro ARCOS Ametek®). The speciation organic/inorganic of TDP was determined from ICP-MS
205 and IC analysis. DOP was estimated from the difference between TDP, obtained by ICP-MS, and DIP, obtained by ion chromatography.

In the rain samples NO_3 , NH_4 and dissolved inorganic phosphorus (DIP) were also determined using ion chromatography following recovery of the dissolved fraction. Total particulate P (TPP) and dissolved organic P (DOP) were also measured in the rain samples
210 following the protocol used for atmospheric dust (described above). The wet deposition fluxes of dissolved nutrients and particulate fractions were estimated from the measured concentrations in the rain sample, multiplied by total precipitation.

Total precipitation was taken from the total hourly precipitation accumulated during the rain event over the region from the ERA5 hourly data reanalysis (Hersbach et al., 2018). In order
215 to incorporate the regional variability of rainfall, the total precipitation was taken from the total hourly precipitation over a domain whose center is the ship with a radius of 110 km using the ERA5 hourly data reanalysis (Hersbach et al., 2018). ERA 5 data are available on regular latitude-longitude grids at $0.25^\circ \times 0.25^\circ$ resolution (Desboeufs et al., 2021, Table 3). Cumulative precipitation was obtained by considering the value at the center of each grid
220 point over the domain.

2.2.2 Nutrients in the water column

Seawater samples for standard nutrient analysis were filtered online ($< 0.2 \mu\text{m}$, Sartorius Sartrobran-P-capsule with a $0.45 \mu\text{m}$ prefilter and a $0.2 \mu\text{m}$ final filter) directly from the Go-
225 Flo bottles (TMC-rosette). Samples collected in acid-washed polyethylene bottles were immediately analyzed on board. Micromolar concentrations of nitrate + nitrite (NO_x) and DIP were determined using a segmented flow analyzer (AAIII HR SealAnalytical©) following Aminot and K erouel (2007) with a limit of quantification (calculated as ten times the standard deviation of ten measurements of the blank) of $0.050 \mu\text{M}$ for NO_x and $0.020 \mu\text{M}$ for DIP.

230 Samples for the determination of nanomolar concentrations of dissolved nutrients were collected in HDPE bottles previously cleaned with supra-pure HCl. For NO_x (primarily NO₃ as the nitrite fraction was mostly negligible), samples were acidified to pH 1 inside the clean container and analyzed back in the home laboratory using a spectrometric method in the visible (540 nm), with a 1 m LWCC (Louis et al., 2015). The detection limit was 6 nM, the
235 limit of quantification was 9 nM and the reproducibility was 8.5%. DIP was analyzed immediately after sampling using the LWCC method after Pulido-Villena et al. (2010), with a detection limit of 1 nM (Pulido-Villena et al., 2021). Total dissolved phosphorus (TDP) and nitrogen (TDN) were measured using the segmented flow analyzer technique after high-temperature (120 °C) persulfate wet oxidation mineralization (Pujo-Pay and Raimbault,
240 1994). DON was obtained as the difference between TDN and NO_x. DOP was obtained as the difference between TDP and DIP. Labile DOP (L-DOP) was estimated as 31% of the DOP values (Pulido-Villena et al., 2021).

Total hydrolysable amino acids (TAAs) were determined as described in detail by Van Wambeke et al. (2021). Briefly, 1 ml of sample was hydrolyzed at 100°C for 20 h with 1 ml
245 of 30% HCl and then neutralized by acid evaporation. Samples were analyzed by high performance liquid chromatography in duplicate according to Dittmar et al. (2009) protocols.

2.2.3 Biological stocks and fluxes in the epipelagic waters

Flow cytometry was used for the enumeration of autotrophic prokaryotic and eukaryotic cells,
250 heterotrophic prokaryotes (hprok) and heterotrophic nanoflagellates (HNF). Water samples (4.5 mL) were fixed with glutaraldehyde grade I 25% (1% final concentration), flash frozen and stored at -80 °C until analysis. Counts were performed on a FACSCanto II flow cytometer (Becton Dickinson). The separation of different autotrophic populations was based on their scattering and fluorescence signals according to Marie et al. (2000). For the
255 enumeration of hprok (Gasol and Del Giorgio, 2000), cells were stained with SYBR Green I (Invitrogen – Molecular Probes). HNF staining was performed with SYBR Green I as described in Christaki et al. (2011). All cell abundances were determined from the flow rate, which was calibrated with TruCount beads (BD biosciences).

Primary production (PP) was determined at 6 layers from the shallow CTD casts (0-250 m)
260 sampled before sun rise. Samples were inoculated with ¹⁴C-bicarbonate and incubated in on-deck incubators kept at in situ temperature by flowing surface seawater and equipped with

various blue screens to simulate different irradiance levels. After 24 h-incubations, samples were filtered through 0.2 polycarbonate filters and treated for liquid scintillation measurement as described in detail in Marañón et al. (2021). A temperature correction was applied as explained in Marañón et al. (2021). N₂ fixation rates (N₂fix) were determined as described in 265 Ridame et al. (2011) using 2.3 L of unfiltered seawater collected in acid-washed polycarbonate bottles and enriched with ¹⁵N₂ gas (99 atom% ¹⁵N) to obtain a final enrichment of about 10 atom% excess. 24 h-incubations for N₂fix were conducted under the same temperature and irradiance as the corresponding PP incubations.

270 To calculate heterotrophic prokaryotic production (BP) samples collected in the epipelagic layers (0-250 m) were incubated with tritiated leucine using the microcentrifuge technique as detailed in Van Wambeke et al. (2021). We used the empirical conversion factor of 1.5 ng C per pmol of incorporated leucine according to Kirchman (1993). Isotope dilution was negligible under these saturating concentrations as periodically checked with concentration 275 kinetics. As we only used 2 on board temperature controlled dark-incubators, a temperature correction was applied as explained in Van Wambeke et al. (2021). Ectoenzymatic activities were measured fluorometrically, using the fluorogenic model substrates L-leucine-7-amido-4-methyl-coumarin (Leu-MCA) and 4-methylumbelliferyl-phosphate (MUF-P) to track aminopeptidase (LAP) and alkaline phosphatase (AP) activity, respectively, as described in 280 Van Wambeke et al. (2021). Briefly, the release of MCA from Leu-MCA and MUF from MUF-P were followed by measuring the increase of fluorescence in the dark (exc/em 380/440 nm for MCA and 365/450 nm for MUF, wavelength width 5 nm) in a VARIOSCAN LUX microplate reader. Fluorogenic substrates were added at varying concentrations (0.025, 0.05, 0.1, 0.25, 0.5 and 1 μM) in 2 ml wells in duplicate. The parameters V_m (maximum hydrolysis velocity) and K_m (Michaelis-Menten constant that reflects enzyme affinity for the substrate) 285 as well as their corresponding errors were estimated by non-linear regression using the Michaelis-Menten equation:

$$V = V_m \times S / (K_m + S)$$

where V is the hydrolysis rate and S the fluorogenic substrate concentration added. We used 290 an approach similar to Hoppe et al. (1993) to compute the *in situ* hydrolysis rates for LAP and AP. We assumed that total amino acids (TAA) could be representative of dissolved proteins. LAP and AP *in situ* activities were thus determined substituting S by TAA and L-DOP *in situ*

concentrations in the Michaelis-Menten equations, respectively (Van Wambeke et al., 2021; Pulido-Villena et al., 2021).

295

2.3. Vertical nutrient fluxes

In the absence of concomitant turbulence measurements, the mixed layer depth (MLD) can be estimated from density profiles (e.g. de Boyer Montegut et al., 2004; D'Ortenzio et al., 2005). For this study, a MLD was determined at every CTD cast as the depth where the residual
300 mass content (i.e., the vertical integral of the density anomaly relative to surface) was equal to 1 kg m^{-2} (Prieur et al., 2020), with an error of estimation of 0.5 m relative to the vertical resolution of the profile (1 m).

In the Mediterranean Sea, the low nutrient availability combined with a shallow mixed layer (ML) lead to the formation of a nutrient depleted layer that extend below the ML. Hereafter,
305 the nutrient depleted layer is referred to 'NDLb' (b for bottom or base) for NO_3 and as PDLb for DIP (Fig. 2). The base of both layers corresponds to the nitracline and phoshacline depths, respectively, estimated by the deepest isopycnal at which measurements of NO_3 and DIP, respectively, reach the detection limit (Kamykowski and Zentara, 1985; Omand and Mahadevan, 2015). Both nitracline and phosphacline depth is estimated at every discrete
310 profile from the intercept of the regression line reported in a nutrient-density diagram. Exchanges of nutrients between the ML and NDLb or PDLb are driven by diffusion or advection (Du et al., 2017). The flux of nutrients is a one dimensional setting and can be expressed as:

$$F_{\text{NO}_3} = F_{\text{DIF}} + F_{\text{ADV}}$$

315 The diffusive flux F_{DIF} is expressed as the gradient of nutrient concentration times a vertical diffusivity coefficient K_z :

$$F_{\text{DIF}} = K_z \times (\text{NO}_3_{\text{ML}} - \text{NO}_3_{\text{NDLb}}) / \text{MLD}$$

The typical magnitude of K_z in the surface layers of the PEACETIME stations was assessed to be $10^{-5} \text{ m}^2 \text{ s}^{-1}$, as discussed in Taillandier et al. (2020).

320 The advective flux F_{ADV} is driven by the entrainment of deeper water in the mixed layer due to the erosion of the near-surface pycnocline, conversely to the detrainment of waters below the mixed layer by restratification, dependent on wind stress and heat flux (Cullen et al., 2002). It is expressed as the variation in the nutrient concentration across the ML times the temporal variation of the MLD, as:

325
$$F_{\text{ADV}} = (\text{NO}_3_{\text{ML}} - \text{NO}_3_{\text{NDLb}}) \times d\text{MLD} / dt$$

Shallow MLs as the ones observed in this study (10 - 20 m) are primarily influenced by wind bursts that can lead to intermittent variations of the MLD, of up to several meters per day (10^5 m s^{-1}). The resulting advective fluxes provide transient exchanges that are one order of magnitude greater than well-established diffusive fluxes. Over the time scale of significant atmospheric deposition events, associated rapid variations of the MLD would rather promote the input of atmospheric nutrients to be exported below the ML by advection rather than by diffusion. In other terms, using the hypothesis of non-stationary regimes due to rapid changes in atmospheric conditions (that control both the mixing state of the ML and atmospheric nutrient inputs), we assume that vertical advection is the main process of exchange.

At short stations, only single casts were carried out, preventing any estimation of temporal variations of the MLD ($d\text{MLD}/dt$) required for the calculation of vertical advective fluxes. Thus only a qualitative assessment of nutrient fluxes across ML is given. Vertical distributions of DIP, along the longitudinal transect, are described in detail in a companion paper (Pulido-Villena et al., 2021).

2.4 Budget from the metabolic fluxes

Trapezoidal integration was used to integrate BP, PP and N_2fix within the ML. The biological activity at the surface was considered to be equal to that of the first layer sampled (around 5 m depth at the short stations, 1 m depth at FAST). When the base of the ML was not sampled, the value at that depth were estimated through linear interpolation between the 2 closest data points above and below the MLD.

For LAP, the transformation of *in situ* rates expressed in $\text{nmol TAA hydrolyzed L}^{-1} \text{ h}^{-1}$ were transformed into nitrogen units using N per mole TAA, as the molar distributions of TAA were available. Integrated *in situ* LAP hydrolysis rates were calculated assuming the Michaelis-Menten parameters V_m and K_m obtained at a 5 m depth to be representative of the whole ML. Thus an average *in situ* volumetric LAP flux in the ML was obtained by combining the average TAA concentrations in the ML with these kinetic parameters, and multiplying this volumetric rate by the MLD. Daily BP, AP and LAP integrated activities were calculated from hourly rates $\times 24$. Assuming no direct excretion of nitrogen or phosphorus, the C/N and C/P ratios of cell demand are equivalent to the cellular ratios. We used molar C/N ratios derived from Moreno and Martiny (2018) (range 6-8, mean 7) for phytoplankton and from Nagata et al. (1986) for heterotrophic prokaryotes (range 6.2-8.4, mean 7.3). C/P of cyanobacteria and picophytoeukaryotes in P depleted conditions ranged

from 107 to 161 (Martiny et al., 2013). Based on these we used a mean C/P of 130 for
360 phytoplankton. A C/P value of 100 was used for heterotrophic prokaryotes (Godwin and
Cotner, 2015).

3. Results

365 3.1 Nutrient patterns and biological fluxes along the PEACETIME transect

During our study, MLD ranged between 7 m (at ST9) and 21 m (at ST1, Table S1, Fig. 3).
The nitracline was shallow in the Provençal Basin (50 – 60 m), 70 m in the Eastern Algerian
and Tyrrhenian Seas; further deepening in the Western Algerian and Ionian Seas (80 - 90 m,
Table S1). Mean NO₃ concentrations in the NDLe ranged from the quantification limit (9
370 nM) to 116 nM (Table S1, Fig. 4). In the ML, mean NO₃ concentrations ranged from 9 to 135
nM. stations were grouped according NO₃ concentrations (Table S1) . Weak gradients, and
therefore low exchange, between the ML and NDLe characterized stations in ‘groups’ 1 to 3.
Stations in ‘group’ 4 showed high and moderate NO₃ concentrations within the ML and
NDLe, respectively, with a large positive difference (> 20 nM) between both layers.

375 At 5 m depth, V_m for leucine aminopeptidase (LAP) ranged from 0.21 to 0.56 nmol MCA-leu
hydrolyzed l⁻¹ h⁻¹, and K_m from 0.12 to 1.29 μM. The mean TAA within the ML ranged from
0.17 to 0.28 μM. The mean *in situ* LAP hydrolysis rate within the ML, derived from these
parameters, ranged from 0.07 to 0.29 nmol N l⁻¹ h⁻¹ (results not shown but detailed in Van
Wambeke et al., 2021).

380 The vertical distributions of PP and BP for the short stations are described in Marañon et al.
(2021). Briefly, PP exhibited a deep maximum close to the DCM depth or slightly above
whereas vertical distribution of BP generally showed 2 maxima, one within the mixed layer,
and a second close to the DCM. Integrated PP (Table 1, Table S2) ranged from 138 (TYR17
May) to 284 (SD1) mg C m⁻² d⁻¹. Integrated BP (0-200 m) ranged from 44 (ION27May) to
385 113 (FAST+0.53) mg C m⁻² d⁻¹. Overall, at the time of the PEACETIME cruise, the transect
exhibited the typical west-east gradient of increasing oligotrophy detected by ocean colour
(see Fig. 8 in Guieu et al., 2020),

3.2 N budgets and fluxes at short stations

390 Biological rates (all expressed in N units) within the ML at the short stations are shown in
Table 2. Phytoplankton N demand (phytoN demand) was the largest, followed by that of

heterotrophic prokaryotes (hprokN demand). On average, phytoN demand was 2.9 (range 1.5 – 8.1) times greater than hprokN demand. LAP hydrolysis rates represented 14 to 66 % of the hprokN demand (mean \pm sd : 37% \pm 19%), N₂ fixation rates represented 1 to 4.5% of the phytoN demand (2.6% \pm 1.3%) and 3 to 11% of the hprok N demand (6.4% \pm 2.4%). N₂ fixation rates integrated over the ML correlated slightly better with hprokN demand ($r = 0.75$) than with phytoN demand ($r = 0.66$).

Dissolved inorganic N (DIN=NO₃+NH₄) solubilized from dry atmospheric deposition ranged from 17 to 40 $\mu\text{mol N m}^{-2} \text{d}^{-1}$ with an average contribution of NO₃ by 79% (Table 2). This new DIN input was similar or higher than N₂ fixation rates within the ML (from 1.3 to 11 fold, mean 4.8-fold). On average, DIN from dry deposition represented 27% of the hprokN demand (range 10-82%) and 11% of the phytoN demand (range 1-30%) within the ML.

3.3 Biogeochemical evolution at ION

The ION site was occupied from May 25 to 29. Rain events in the vicinity of the ship were observed on May 26 and May 29 (Desboeufs et al., 2021). On May 29 the rain event was associated with a rain front extending over more than 5 000 km². A rain sample could be taken on board on May 29th between 5:08 and 6:00 (local time), i.e. just 3 hours before the last CTD cast. The chemical composition of the rain indicated an anthropogenic origin (Desboeufs et al., 2021).

TDP solubilized from dry atmospheric deposition decreased from 268 nmol P m⁻² d⁻¹ (May 25 - 26) to 124 nmol P m⁻² d⁻¹ (May 27-28). DIN fluxes from dry atmospheric deposition averaged 29 \pm 4 $\mu\text{mol N m}^{-2} \text{d}^{-1}$ with small variability during the occupation of the site (Table S2). The molar ratio of DIN/DIP in the rain was 208 and DOP represented 60% of the total dissolved P (Table 3).

CTD casts were taken each 24 h for biological fluxes or every 48 h for DIP and NO₃. Thus the temporal evolution for nutrients in the water column at ION is given only by three profiles. The first profile (May 25 before the rain events in the area) made during smooth weather conditions shows a shallow ML with low and homogeneous concentrations of NO₃ in the ML and the NDLe (Fig. 4). Shortly after, rain events were observed in the area on May 26 although not at the ship's position and the ML started to deepen 13 h before the second cast sampled for nutrients (on May 27) and NO₃ concentrations increases in the ML and NDLe Fig. 3). While NO₃ concentrations increased in the ML, the effect on the MLD was

425 still moderate as wind conditions rose to 20 kt just at the time of the cast (Fig. 3). The interval
between the second and the third cast (May 29, cast done 3 hours after the rain sampled on
board) was marked by a slight decrease in wind speed, a deepening of the ML down to 18 m
and a decrease in NO₃ both in the ML and NDLe, with comparatively higher NO₃
430 concentrations in ML than in the NDLe. The calculation of vertical advective fluxes between
the two layers showed a downward flux in the first interval May 25-27 (Fig. 4, Table S1) and
an upward flux in the second interval (May 27-29).

Due to the lack of high frequency sampling, it was not possible to quantitatively assess the
effects of dry/wet atmospheric deposition nor the one of nitrate injection from below the
NDLe by vertical advection at ION. The intrusion of a low-salinity lens was clearly visible on
435 the thermosalinograph record and on the 27 May CTD cast, down to 10 m depth (data not
shown). This low-salinity lens could be formed by the rain event noted on 26 May in the
vicinity of the station. It was clear that ION on days May 27 and 29 was characteristic of
group 4 (i.e. higher NO₃ concentrations in the ML than in the NDLe), presumably related to
NO₃ rainfall inputs. V_m of LAP measured on May 25 at 5 m (0.22 nmol N l⁻¹ h⁻¹) was one of
440 the lowest values recorded during the cruise whilst V_m of AP was the highest (5.6 nmol P l⁻¹
h⁻¹). PP integrated over the euphotic zone increased slightly from 188 to 226 mg C m⁻² d⁻¹
(Table S2), but due to the variability in the MLD at ION this trend was not visible when
integrating PP over the ML. In the ML, BP increased slightly, from 7.5 to 10.3 mg C m⁻² d⁻¹
445 between May 25 and May 29, indicating that hprok benefited slightly more from the
atmospheric inputs than the autotrophs (Fig. S1, Table S2). The profiles of hprok and
Synechococcus abundances showed no particular trend with time, with larger variations
within the DCM (Fig. S1).

3.4 N budgets and fluxes at FAST

450 During the occupation of FAST, two rains episodes took place starting on the evening of June
2 to the June 3 at night and in the early morning of June 5 (Tovar-Sanchez et al., 2020). The
radar data indicated the presence of a rain front with patchy, numerous and intense rain events
occurring over a large area surrounding the ship's location. These two episodes coincided
with a dust plume transported in altitude (between 1 and 4 km) and resulted in wet deposition
455 of dust (Desboeufs et al., 2021). A rain sample was collected on board on June 5th (between
02:36 and 03:04, local time) and was associated with a dust wet deposition flux of ~ 40 mg m⁻².
The DIN/DIP ratio in the rain reached 480 (Table 3). After the rain, daily fluxes of DIN

solubilized from dry aerosol deposition strongly decreased from 61.2 to 12.9 $\mu\text{mol N m}^{-2} \text{d}^{-1}$ between June 4 and 5.

460

The water column at FAST site before the rain event sampled on board (-2.3; -1.5; -0.25 days) was marked by moderate and similar decreases in NO_3 concentrations within the ML and ND**L**b. Integrated NO_3 stocks in the ML (Table S2) reflected slight changes in MLD (from 14 to 10 m during this time interval). On June 5th, the rain event (Table 3) was associated with a strong wind burst and an abrupt mixing. The comparison between NO_3 concentrations from two casts, sampled 6 h before and 6 h after the rain, (FAST-0.25 and FAST+0.24), showed a clear N enrichment of the ML with a mean NO_3 increase from 56 to 93 nM corresponding to a NO_3 integrated stocks increase by 888 $\mu\text{mol N m}^{-2}$ (Fig. 3, Table S2). There was also a clear difference in the mean NO_3 concentrations between ML and ND**L**b (93 ± 15 vs 51 ± 7 nM, respectively). This is the largest NO_3 difference observed during the cruise between these 2 layers (Fig. 4), confirming that the ML enrichment could not be attributed to inputs from below. The relaxation of the wind burst was progressive, with a continuous deepening of the ML (Table S1). The export of the atmospheric NO_3 into the ND**L**b was highest after the rain event (FAST+0.24). At the end of the FAST occupation period (FAST+3.8) high NO_3 concentrations (mean 135 nM) were measured again within the ML.

475

DIP concentration dynamics were different from those of NO_3 , with similar DIP integrated stocks within the ML being measured 6 h before and 6 h after the rain (136 $\mu\text{mol P m}^{-2}$). From then on, DIP stocks progressively increased reaching a maximum (281 $\mu\text{mol P m}^{-2}$) one day after the rain (FAST+1).

480

Immediately after the rain, integrated PP (euphotic zone) decreased from 274 $\text{mg C m}^{-2} \text{d}^{-1}$ (FAST-0.9) to 164 $\text{mg C m}^{-2} \text{d}^{-1}$ (FAST+0.07) and continued to decrease the following day. It was only 3.8 days after the rain that PP returned to initial values (Table S2). Such variations were mostly due to changes in PP within the DCM depth (Fig. S2), as the values did not change significantly within the ML (28-33 $\text{mg C m}^{-2} \text{d}^{-1}$, Fig. S2, Fig. 5). Integrated BP in the upper 200 m of the water column showed the opposite trend to that of PP, increasing from 86 ± 3 $\text{mg C m}^{-2} \text{d}^{-1}$ ($n = 4$) before the rain, up to 113 $\text{mg C m}^{-2} \text{d}^{-1}$ at FAST+0.5, (Table S2).

485

Although modest, this increasing trend was also visible over the ML (12-15 to 15-19 $\text{mg C m}^{-2} \text{d}^{-1}$ after the rain event). The abundances of picophytoplankton groups varied mostly in the vicinity of the DCM depth with peaks occurring 1-2 days after the rain (grey profiles, Fig S3),

490 in particular for prokaryotes (*Prochlorococcus*, *Synechococcus*). Heterotrophic prokaryotes and nanoflagellate abundances increased slightly within the DCM depth after the rain.

4. Discussion

495 The specific context of the oceanographic survey constrained the temporal and spatial coverage of our analysis, as the biogeochemical responses to a rain event were investigated over a few days (3 - 5), and tens of km (40 - 50). Their evolution was restricted to the vertical dimension, integrating lateral exchanges by horizontal diffusion or local advection that occurred over the corresponding space and time scales. In the vertical dimension, exchanges
500 of nutrients across the ML were controlled by mixing due to rapidly changing conditions (MLD fluctuations along with nutrient inputs from the atmosphere) rather than diffusion. Four groups of stations, corresponding to different stages of ML enrichment and relaxation, due to the nutrient inputs from single rain events, have been characterized based on the differences in NO₃ concentration between the ML and NDLb (see section 2.4). As shown in Fig. 4, this
505 succession of stages is in agreement with the NO₃ fluxes from above and below the ML. Moreover, they provide a temporal scaling of the oceanic response to atmospheric deposition, with a quasi-instantaneous change at the time of the rain event and a 2-day relaxation period to recover to pre-event conditions

In this context, we will i) discuss the nitrogen budget within the ML at the short stations
510 considered as a 'snapshot', and ii) analyze in detail, using a time series of CTD casts, the biogeochemical changes within the ML and the NDLb following the atmospheric wet deposition event at FAST, discussing the possible modes of transfer of nutrients between these 2 layers.

515 **4.1 A snapshot of biological fluxes in the ML and their link to new DIN from atmospheric dry deposition**

The dependence of hprok on nutrients rather than on labile organic carbon during stratification conditions is not uncommon in the MS (Van Wambeke et al., 2002, C ea et al, 2017; Sala et al., 2002) and has also been shown during PEACETIME cruise (P, or N,P
520 colimitation, Fig. S4). Hprok have an advantage due to their small cell size and their kinetic systems which are adapted to extremely low concentrations of nutrients (for example for DIP see Talarmin et al., 2015). Under such conditions of limitation, hprok will react rapidly to

new phosphorus and nitrogen inputs, coming from atmospheric deposition. During an artificial *in situ* DIP enrichment experiment in the Eastern Mediterranean, P rapidly circulated through hprok and heterotrophic ciliates, and the phytoplankton was not directly linked to this 'bypass' process (Thingstad et al., 2005). Bioassays conducted in the tropical Atlantic Ocean have also shown that hprok respond more strongly than phytoplankton to nutrients from Saharan aerosols (Marañón et al. 2010), a pattern that has been confirmed in a meta-analysis of dust addition experiments (Guieu et al., 2014; Guieu and Ridame, in press; Gazeau et al., 2021).

We considered hprokN demand together with phytoN demand and compared it to autochthonous (DON hydrolysis by ectoenzymatic activity) and allochthonous (atmospheric deposition) sources. To the best of our knowledge this is the first time that these fluxes are compared based on their simultaneous quantification at sea. High variability was observed among the 10 short stations (Table 2). The regeneration of nitrogen through aminopeptidase activity was clearly the primary provider of N to hprok as 14 to 66% (mean \pm sd : 37% \pm 19%) of the hprokN demand could be satisfied by *in situ* LAP activity. Such percentages may be largely biased by the conversion factors from C to N and propagation of errors for the LAP hydrolysis rates and BP rates. However, the C/N ratio of hprok is relatively constant even under large variations of P or N limitation (6.2 to 8.4; Nagata, 1986).

Other regeneration sources exist such as direct excretion of NH₄ or low molecular weight DON sources with no necessity for hydrolysis prior to uptake (Jumars et al., 1989). For instance, Feliú et al. (2020) calculated that NH₄ and DIP excretion by zooplankton would satisfy 25-43% of the phytoN demand and 22-37% of the phytoP demand over the whole euphotic zone. Such percentages suggest that direct excretion by zooplankton along with ectoenzymatic activity provide substantial N for biological activity.

N₂ fixation is also a source of new N that can directly fuel hprok as some diazotrophs are heterotrophic (Delmont et al. 2018, and references therein), or indirectly, as part of the fixed N₂ that rapidly cycles through hprok (Caffin et al., 2018). Furthermore, it has been observed that there is a better coupling of N₂fixation rates with BP rather than with PP in the eastern MS (Rahav et al., 2013b). This was also observed within the ML in this study. Our data showed that the hypothetical contribution of N₂fixation rates to hprokN demand within the ML was low (6.4 \pm 2.4%) and consistent with the low N₂fixation rates observed in the MS (i.e. Rahav et al., 2013a; Ibello et al., 2010; Ridame et al., 2011; Bonnet et al., 2011). This differs

from other parts of the ocean primarily limited by N but not by P, such as the south eastern Pacific where N₂ fixation rates are high (Bonnet et al., 2017) and can represent up to 81 % of the hprokN demand (Van Wambeke et al., 2018).

The sum of LAP activity and N₂ fixation were not sufficient to meet hprokN demand (total contribution between 19 to 73% of HbactN demand). We examined the importance of new
560 DIN from dry atmospheric deposition. Atmospheric DIN fluxes from dry deposition showed a low variability along the transect ($29 \pm 7 \mu\text{mol N m}^{-2} \text{d}^{-1}$ at the short stations) and were among the lowest previously measured in the Mediterranean basin, ranging from 38 to 240 $\mu\text{mol N m}^{-2} \text{d}^{-1}$ (Desboeufs, in press). It has to be noted that the fluxes measured during the
565 PEACETIME cruise are representative of the open sea atmosphere while published fluxes were measured at coastal sites where local/regional contamination contributes significantly to the fluxes (Desboeufs, in press). Atmospheric deposition also delivers organic matter (Djaoudi et al., 2017, Kanakidou et al., 2018), which is bioavailable for marine hprok (Djaoudi et al., 2020). Dissolved organic nitrogen (DON) released from aerosols, not
570 determined here, can be estimated from previous studies. On average in the MS, DON solubilized from aerosols represents 32%. (range 19 to 42%) of the total dissolved N released from dry deposition (Desboeufs, in press). Considering this mean, DON released from dry deposition was estimated to range from 8 to 19 $\mu\text{mol N m}^{-2} \text{d}^{-1}$ at the short duration stations. The total dissolved N solubilized from dry deposition (inorganic measured +organic
575 estimated) would thus represent 14 to 121% of the hprokN demand. Because of the low variability in DIN (and estimated DON) fluxes derived from dry deposition, the atmospheric contribution was mainly driven by biogeochemical processes in the water column and not by the variability of atmospheric fluxes during the cruise (CV of Nprok Ndemand and phyto N demand at the short stations were 45% and 89%, respectively, and that of DIN flux 25%).
580 However, the calculated contribution can also be biased by the deposition velocity used to calculate DIN solubilized from the dry deposition. Deposition velocity was set at 1 cm s^{-1} for NO₃ and 0.21 cm s^{-1} for NH₄. As NO₃ was the dominant inorganic form released by dry deposition, it is clear that the choice of 1 cm s^{-1} for NO₃ influenced its contribution. This choice was conditioned by the predominance of NO₃ in the main types of aerosols in the
585 Mediterranean basin such as dust or sea salt particles (e.g., Bardouki et al., 2003). However, the deposition velocity of NO₃ between fine and large particles could range from 0.6 to 2 cm sec^{-1} in these aerosols (e.g. Sandroni et al., 2007). Even considering the lower value of 0.6 $\text{cm$

sec⁻¹ from the literature, the contribution of DIN from atmospheric dry deposition to hprokN demand within the ML would still be significant (up to 72%).

590

4.2 Biogeochemical response after a wet deposition event – N and P budgets at FAST

Rain events are more sporadic than dry atmospheric deposition but represent much higher new nutrient fluxes to the MS surface waters on an annual basis, e.g. on average 84% of annual atmospheric DIN fluxes in Corsica Island (Desboeufs et al., 2018). At the scale of the Mediterranean basin, the annual wet deposition of DIN was found to be 2-8 times higher than DIN from dry deposition (Markaki et al., 2010). Wet deposition also contributes significantly to DON atmospheric fluxes in the MS: For example at Frioul Island (Bay of Marseille, NW MS), total (wet + dry) DON atmospheric fluxes ranged between 7 and 367 $\mu\text{mol DON m}^{-2} \text{ day}^{-1}$ and represented $41 \pm 14\%$ of the total atmospheric nitrogen flux (Djaoudi et al., 2018). In the Eastern MS (Lampedusa Island) DON atmospheric fluxes ranged between 1.5 and 250 $\mu\text{mol DON m}^{-2} \text{ day}^{-1}$ contributing 25% of the total atmospheric nitrogen flux, respectively (Galletti et al., 2020). In both studies, bulk atmospheric fluxes of DON were positively correlated with precipitation rates, indicating the preponderance of wet over dry deposition.

At FAST, the maximum net variations of NO₃ and DIP concentrations within the ML before/after the rainy period reached 1520-665 = +855 $\mu\text{mol N m}^{-2}$ for NO₃ and 281-137 = +144 $\mu\text{mol P m}^{-2}$ for DIP (Table S2). In other terms, based on a mean MLD of 16 m, the net observed increases in the ML were +9 nM DIP and +54 nM NO₃. These net variations observed in the ML are higher than the calculated variation in stocks deduced from the N and P concentrations of this rain event (0.07 nM DIP and 21 nM NO₃ concentrations increase over the whole ML (Table 3). This is still true when including all P or N chemical species (particulate and soluble inorganic + organic fractions) with, for example an increase in P concentration in the ML of ~0.68 nM. As described in the results section 3.4, the rains affecting the FAST site were spatially patchy over a large area (~40-50 km radius around the R/V). Thus, we consider that the biogeochemical impacts observed at FAST site were probably due to a suite of atmospheric events rather than only the single event observed on board. It is also possible that meso- and sub-mesoscale dynamics encountered at FAST site (Figs 5 and 12 in Guieu et al., 2020) may have affected such cumulative impact.

Interestingly, a delay of about 19 h was observed in the maximum net accumulation within the ML between DIP (FAST+1.05) and NO₃ (FAST+0.24). The DIN/DIP ratio in the rain

620

(1438) was much higher than the Redfield ratio. As the biological turnover of DIP in the MS is rapid (from minutes to few hours, Talarmin et al., 2015), new DIP from rain might have behaved differently than DIN. Two different mechanisms can explain this delay: (i) processes linked to bypasses and luxury DIP uptake (storage of surplus P in hprok before a rapid
625 development of grazers (Flaten et al, 2005; Herut et al 2005, Thingstad et al., 2005) that are later responsible for DIP regeneration) so that DIP net accumulation is delayed and/or (ii) abiotic processes such as rapid desorption from large sinking particles followed by adsorption of DIP onto submicronic iron oxides still in suspension as observed experimentally in Louis et al. (2015).

630 The first proposed mechanism may be supported by the observed increase of BP, along with a stable PP which suggests an immediate benefit of the new nutrients from rain to hprok rather than phytoplankton. The so-called luxury DIP uptake by organisms like hprok is efficient (small cells with high surface/volume ratio and DIP kinetic uptake adapted to low concentrations). It is of course difficult to quantify such *in situ* variations in comparison to
635 mesocosms/minicosms dust addition experiments, in which clearly heterotrophy was promoted (Marañón et al., 2010; Guieu et al., 2014b; Gazeau et al., 2021). Few field studies have confirmed these trends (Herut et al., 2005, Pulido-Villena et al., 2008) but, as stated in the introduction, these studies lacked high frequency sampling.

The second proposed mechanism, the abiotic desorption/adsorption, is compatible with the
640 observed 19 h delay (Louis et al., 2015). Note that most of the estimates of such abiotic processes are from dust addition experiments with contrasting results, some showing this abiotic process of absorption/desorption while the particles are sinking (Louis et al., 2015), and others not (Carbo et al., 2005; Ridame et al., 2003). It is possible that DIP adsorbed onto large particles rapidly sinks out of the ML, and desorbs partly during its transit in the PDLb,
645 where it could remain for longer periods due to the stratification at the pycnoclines.

We made a tentative P budget between FAST+1.05 and FAST+2.11 where a net ML decrease in DIP ($-87 \mu\text{mol P m}^{-2}$) was observed. During this time, advective flux of DIP into the PDLb was not detectable as DIP concentrations within the ML were always lower than within the PDLb (Pulido-Villena et al., 2021.). This indicated that DIP was assimilated and/or
650 transformed to DOP via biological processes, and/or adsorbed onto particles and exported to PDLb by sedimentation. By integrating PP and BP over this period (34.5 and 19.7 mg C m^{-2} , respectively) and assuming that the $87 \mu\text{mol DIP m}^{-2}$ removed were consumed by hprok and phytoplankton, the C/P ratio of their biomass would be 52. Such C/P suggests that DIP was

not limiting these organisms anymore. Indeed a decrease of C/P quotas may highlight a
655 switch from P to C limitation for heterotrophic bacteria (Godwin and Cotner, 2015) and from
P to N limitation or increased growth rates for phytoplankton (Moreno and Martiny, 2018).
Furthermore, as DIP is also recycled via alkaline phosphatase within the ML, we also
consider another source of DIP via alkaline phosphatase activity, which could release 139
 $\mu\text{mol DIP m}^{-2}$ during this period (see Van Wambeke et al., 2021 for *in situ* estimates).
660 Assuming also that DIP resulting from AP hydrolysis was fully assimilated by the plankton,
the C/P ratio would be 19. This low ratio seems unrealistic for phytoplankton (Moreno and
Martigny, 2018) as well as hprok, even growing in surplus C conditions (Makino et al., 2003;
Lovdal et al., 2008; Godwin and Cotner, 2015).
Some of the P recycled or brought into the ML from atmospheric deposition has consequently
665 been exported below the ML. DIP is abiotically adsorbed on mineral dust particles (Louis et
al., 2015), and is exported out of the ML while particle sedimentation. It is also possible that
such processes enable the export of other P-containing organic molecules, such as DOP or
viruses produced following luxury DIP assimilation. Free viruses, richer in P than N relative
to Hprok, could adsorb, like DOM, onto dust particles and constitute a P export source.
670 Indeed, free viruses adsorb onto black carbon particles, possibly reducing viral infection
(Mari et al., 2019; Malits et al., 2015). However, particle quality is a determining factor for
DOM or microbial attachment, and what has been shown for black carbon particles is not
necessarily true for dust particles. For instance, the addition of Saharan dust to marine coastal
waters led to a negligible sorption of viruses to particles and increased abundance of free
675 viruses (Pulido-Villena et al., 2014), possibly linked to an enhancement of lytic cycles in the
ML after relieving limitation (Pradeep Ram and Sime-Ngando, 2010).
We are aware of all the assumptions made here, including (i) conversion factors, (ii) *in situ*
estimates of alkaline phosphatase, (iii) some missing DIP sources in the budget, such as the
excretion of zooplankton estimated to amount to 22-37% of the phytoP demand at FAST site
680 (Feliú et al., 2020), (iv) lack of knowledge on the different mechanisms linking P to dust
particles, and (v) considering the station as a 1D system. Nevertheless, all these results
together suggest that both luxury consumption by Hprok and export via scavenging on
mineral particles probably occurred simultaneously and could explain the observed variations
of DIP in the ML.

685

For NO₃, and in contrast to the observations for DIP, we observed physical exchanges by advection between the ML and NDLe. A N budget within the ML during the period of net NO₃ decrease (between FAST+0.24, and FAST+2.11, Table S2), indicates a net loss of 1343 $\mu\text{mol N m}^{-2}$. For this period lasting 1.8 days, the time-integrated phytoN and hprokN demands were 682 $\mu\text{mol N m}^{-2}$ and 378 $\mu\text{mol N m}^{-2}$, respectively, so that total biological demand in the ML was 1060 $\mu\text{mol N m}^{-2}$. During this period, the possible N sources used were NO₃ which decreased by 1343 $\mu\text{mol N m}^{-2}$ as well as N₂ fixation = 13 $\mu\text{mol N m}^{-2}$ and *in situ* aminopeptidase activity = 87 $\mu\text{mol N m}^{-2}$. In total, these possible sources of N amounted to 1443 $\mu\text{mol N m}^{-2}$. Keeping in mind that the same potential caveats mentioned for DIP (see above) also apply for N budget, the biological N demand appeared lower than the sources (difference $\sim 380 \mu\text{mol N m}^{-2}$). On the other hand, at FAST, vertical advective fluxes of NO₃ from ML to NDLe were up to 337 $\mu\text{mol N m}^{-2} \text{ d}^{-1}$ (Fig. 4), i.e. $\sim 600 \mu\text{mol N m}^{-2}$ was lost from the ML over 1.8 days. From these two different approaches, exported NO₃ should range between 380 and 600 $\mu\text{mol N m}^{-2}$ over this period. Thus, about 40% of the NO₃ accumulated in the ML after the rain was likely exported by vertical advection to the NDLe. Organisms present in the DCM could benefit of this input of new nutrients. Indeed, PP and abundances of all 4 phytoplankton groups (*Synechococcus*, *Prochlorococcus*, nano and picoeukaryotes) increased at the DCM after 24h and remained high for 2 days after the rain event (Fig. S3). The increase in abundances were higher for prokaryotic phytoplankton abundances, as such organisms would likely benefit from their small size and their ability to use DON/DOP from organic molecules (Yelton et al., 2016).

5. Conclusions

This study reports for the first time, in the context of an oceanographic cruise, simultaneous sampling of atmospheric and ocean biogeochemical parameters to characterize the *in situ* biogeochemical responses to atmospheric deposition within the ML. High-frequency sampling, in particular at FAST, confirmed the transitory state of exchanges between the ML and the NDLe. Even if dry deposition measured along the transect was homogeneous and amongst the lowest observed in the MS, that input could represent up to 121% of the hprokN demand.

Our results have shown the important role played by the ML in the biogeochemical and physical processes responsible for transfers of nutrients between the atmosphere and the

nutrient depleted layer below. Thanks to the use of the LWCC technique and access to
nanomolar values of NO₃ and DIP in repeated CTD casts, it was possible to demonstrate the
720 role of the ML and exchanges of NO₃ from the ML to the NDLe by vertical advection when
variations of MLD occurred simultaneously to transitory accumulation of NO₃ after a
deposition event. The time sequence occurring after a wet dust deposition event was
summarized as follows (Fig. 6) : accumulation of NO₃ in the ML, advection to NDLe, luxury
consumption of DIP by hprok and delayed peaks of DIP, decrease of primary production and
725 subsequent recovery after 2 days, mainly visible in the nutrient depleted layer. Dust
deposition triggers a complex and time-controlled trophic cascade within the microbial food
web. Our study shows the important role of intermittent, but strong abiotic effects such as
downwelling advective fluxes from the ML to the nutrient depleted layers. It will be
important to consider these aspects in biogeochemical budgets and models, especially when
730 climate and anthropogenic changes are predicted to increase aerosol deposition in the
Mediterranean Sea.

Data availability

Guieu et al., Biogeochemical dataset collected during the PEACETIME cruise. SEANOE.
<https://doi.org/10.17882/75747> (2020).

735

Author contribution

CG and KD designed the study. FVW measured ectoenzymatic activity and BP, AE
managed the TAA analysis and treatments, EP measured DIP with the LWCC technique,
CR measured nitrogen fixation, VT assisted in CTD operations and analyzed water
740 masses, JD sampled for DOC and flow cytometry, EM analyzed the primary production
data, FVW prepared the ms with contribution from all co-authors.

Competing interests

The authors declare that they have no conflict of interest.

745

Special issue statement

This article is part of the special issue ‘Atmospheric deposition in the low-nutrient–low-
chlorophyll (LNLC) ocean: effects on marine life today and in the future (ACP/BG inter-
journal SI)’. It is not associated with a conference.

Financial support

The project leading to this publication received funding from CNRS-INSU, IFREMER, CEA, and Météo-France as part of the program MISTRALS coordinated by INSU (doi: 10.17600/17000300) and from the European FEDER fund under project no 1166-39417.

755 The research of EM was funded by the Spanish Ministry of Science, Innovation and Universities through grant PGC2018-094553B-I00 (POLARIS).

Acknowledgements. This study is a contribution of the PEACETIME project (<http://peacetime-project.org>, last access 23/09/2021), a joint initiative of the MERMEX

760 and ChArMEx components. PEACETIME was endorsed as a process study by GEOTRACES and is also a contribution to IMBER and SOLAS international programs.

The authors thank also many scientists & engineers for their assistance with sampling/analyses: Samuel Albani for NO₃ nanomolar sampling and Maryline Montanes for NO₃ with LWCC technique, Marc Garel, Sophie Guasco and Christian Tamburini for ectoenzymatic activity, Ruth Flerus and Birthe Zäncker for TAA, Joris Guittoneau and Sandra Nunige for nutrients, Thierry Blasco for POC, Julia Uitz and Céline Dimier for TChl a (analysed at the SAPIG HPLC analytical service at the IMEV, Villefranche), María Pérez Lorenzo for primary production measurements, Philippe Catala for flow cytometry analyses, Barbara Marie and Ingrid Obernosterer for DOC analyses and treatments, Sylvain Triquet and Franck Fu for atmospheric particulate nitrogen and phosphorus and PEGASUS team for atmospheric sampling. Maurizio Ribera d'Alcala and a second anonymous reviewer helped much to improve this ms. We warmly thank the Co-Editor in Chief, Cristine Klass for her corrections which greatly improved the lecture of this ms.

775 References

Aminot, A., and Kérouel, R. : Dosage automatique des nutriments dans les eaux marines, in: Méthodes d'analyses en milieu marin, edited by: IFREMER, Plouzané, 188 pp, IBSN no 978-2-7592-0023-8, 2007.

780 Bardouki, H., Liakakou, H., Economou, C., Sciare, J., Smolik, J., Zdimal, V., Eleftheriadis, K., Lazaridis, M., Dye, C., and Mihalopoulos, N.: Chemical composition of size

- resolved atmospheric aerosols in the eastern Mediterranean during summer and winter, *Atmos. Environ.*, 37, 195–208, 2003.
- 785 Bonnet, S., Grosso, O., and Moutin, T.: Planktonic dinitrogen fixation along a longitudinal gradient across the Mediterranean Sea during the stratified period (BOUM cruise), *Biogeosciences*, 8, 2257–2267, 2011.
- Bonnet, S., Caffin, M., Berthelot, H., and Moutin, T.: Hot spot of N₂ fixation in the western tropical South Pacific pleads for a spatial decoupling between N₂ fixation and denitrification, *PNAS letter*, doi: 10.1073/pnas.1619514114, 2017.
- 790 Caffin, M., Berthelot, H., Cornet-Barthaux, V., Barani, A., and Bonnet, S.: Transfer of diazotroph-derived nitrogen to the planktonic food web across gradients of N₂ fixation activity and diversity in the western tropical South Pacific Ocean, *Biogeosciences*, 15, 3795–3810, doi: 10.5194/bg-15-3795-2018, 2018.
- 795 Carbo, P., Krom, M. D., Homoky, W. B., Benning, L. G., and Herut, B.: Impact of atmospheric deposition on N and P geochemistry in the southeastern Levantine basin, *Deep Sea Res. II*, 52, 3041–3053. doi: 10.1016/j.dsr2.2005.08.014, 2005.
- 800 Céa, B., Lefèvre, D., Chirurgien, L., Raimbault, P., Garcia, N., Charrière, B., Grégori, G., Ghiglione, J.-F., Barani, A., Lafont, M., and Van Wambeke, F.: An annual survey of bacterial production, respiration and ectoenzyme activity in coastal NW Mediterranean waters: temperature and resource controls, *Environ. Sci. Pollut. Res.*, doi: 10.1007/s11356-014-3500-9, 2014.
- Christaki, U., Courties, C., Massana, R., Catala, P., Lebaron, P., Gasol, J. M., and Zubkov, M.: Optimized routine flow cytometric enumeration of heterotrophic flagellates using SYBR Green I, *Limnol. Oceanogr. Methods*, 9, doi: 10.4319/lom.2011.9.329, 2011.
- 805 Cullen, J. J., Franks, P. J., Karl, D. M., and Longhurst, A. L. A. N.: Physical influences on marine ecosystem dynamics. *The sea*, 12, 297-336, 2002.
- de Boyer Montegut, C., Madec, G., Fisher, A. S., Lazar, A., and Iudicone, D.: Mixed layer depth over the global ocean: An examination of profile data and a profile-based climatology, *Journal of Geophysical Research. Oceans*, 109, C12003, doi: 10.1029/2004JC002378, 2004.

- 810 Delmont , T. O., Quince, C., Shaiber, A., Esen, Ö. C., Lee, S. T. M., Rappé, M. R., McLellan, S. L., Lückner, S. and Murat Eren, A.: Nitrogen-fixing populations of Planctomycetes and Proteobacteria are abundant in surface ocean metagenomes, *Nature Microbiology*, doi: 10.1038/s41564-018-0176-9, 2018.
- 815 Desboeufs, K.: Nutrients atmospheric deposition and variability, in: *Atmospheric Chemistry and its Impacts in the Mediterranean Region, volume 2 – From Air pollutants Sources to Impacts*, Dulac, F., Sauvage, S., Hanoumou, E., Eds, Springer, Switzerland, IBSN 978-3-030-82385-6, Chapter 16, in press.
- 820 Desboeufs, K., Bon Nguyen, E., Chevaillier, S., Triquet, S., and Dulac, F.: Fluxes and sources of nutrient and trace metal atmospheric deposition in the northwestern Mediterranean, *Atmospheric Chemistry and Physics*, 18, 14477–14492, doi: 10.5194/acp-18-14477-2018, 2018.
- 825 Desboeufs, K., Fu, F., Bressac, M., Tovar-Sánchez, A., Triquet, S., Doussin, J-F., Giorio, C., Chazette, P., Disnaquet, J., Feron, A., Formenti, P., Maisonneuve, P., Rodríguez-Romero, A., Zapf, P., Dulac, F., and Guieu, C.: Wet deposition in the remote western and central Mediterranean Sea as a source of trace metals to surface seawater, *Atmos. Chem. Phys. Discuss.* [preprint], <https://doi.org/10.5194/acp-2021-624>, in review, 2021.
- Dittmar, T.H., Cherrier, J., and Ludwichowski, K.-U: The analysis of amino acids in seawater. In: *Practical Guidelines for the Analysis of Seawater*, edited by: Wurl, O., Boca Raton, FL: CRC-Press, 67–78, 2009.
- 830 D'Ortenzio, F., Iudicone, D., de Boyer Montegut, C., Testor, P., Antoine, D., Marullo, S., Santoleri, R., and Madec, G.: Seasonal variability of the mixed layer depth in the Mediterranean Sea as derived from in situ profiles., *Geophysical Research Letters*, 32, L12605, doi:10.1029/2005GL022463, 2005.
- 835 Djaoudi, K., Van Wambeke, F., Barani, A., Hélias-Nunige, S., Sempéré, R., and Pulido-Villena, E.: Atmospheric fluxes of soluble organic C, N, and P to the Mediterranean Sea: potential biogeochemical implications in the surface layer, *Progress in Oceanography*, 163: 59-69, MERMEX special issue, doi: 10.1016/j.pocean.2017.07.008, 2017.

- 840 Djaoudi, K., Van Wambeke, F., Coppola, L., D'ortenzio, F., Helias-Nunige, S., Raimbault, P.,
Taillandier, V., Testor, P., Wagener, T., and Pulido-Villena, E.: Sensitive determination
of the dissolved phosphate pool for an improved resolution of its vertical variability in
the surface layer: New views in the P-depleted Mediterranean Sea, *Frontiers in Marine
Science*, vol 5, article 234, doi: 10.3389/fmars.2018.00234, 2018.
- 845 Djaoudi, K., Van Wambeke, F., Barani, A., Bhairy, N., Chevaillier, S., Desboeufs, K.,
Nunige, S., Labiadh, M., Henry des Tureaux, T., Lefèvre, D., Nouara, A.,
Panagiotopoulos, C., Tedetti, M., and Pulido-Villena E.: Potential bioavailability of
organic matter from atmospheric particles to marine heterotrophic bacteria,
Biogeosciences, 17, 6271–6285, <https://doi.org/10.5194/bg-17-6271-2020>, 2020
- 850 Du, C., Liu, Z., Kao, S.-J., and Dai, M.: Diapycnal fluxes of nutrients in an oligotrophic
oceanic regime: The South China Sea, *Geophysical Research Letters*, 44, 11, 510–11,
518, doi: 10.1002/2017GL074921, 2017.
- 855 Feliú, G., Pagano, M., Hidalgo, P., and Carlotti, F.: Structure and function of epipelagic
mesozooplankton and their response to dust deposition events during the spring
PEACETIME cruise in the Mediterranean Sea, *Biogeosciences*, 17, 5417–5441,
<https://doi.org/10.5194/bg-17-5417-2020>, 2020.
- Flaten, G. A., Skjoldal, E. F., Krom, M. D., Law, C. S., Mantoura, F. C., Pitta, P., Psarra, S.,
Tanaka, T., Tselepides, A., Woodward, E. M., Zohary, T., and Thingstad, T. F.: Studies
of the microbial P-cycle during a Lagrangian phosphate-addition experiment in the
Eastern Mediterranean, *Deep-Sea Res II*, 52, 2928–2943, 2005.
- 860 Fu, F., Desboeufs, K., Triquet, S., Doussin, J-F., Giorio, C., and Guieu, C.: Solubility and
sources of trace metals associated with aerosols collected during cruise PEACETIME in
the Mediterranean Sea, *Atmos. Phys. Chem.*, this special issue, in preparation.
- 865 Galletti, Y., Becagli, S., di Sarra, A., Gonnelli, M., Pulido-Villena, E., Sferlazzo, D. M.,
Traversi, R., Vestri, S., and Santinelli, C.: Atmospheric deposition of organic matter at a
remote site in the Central Mediterranean Sea: implications for marine ecosystem,
Biogeosciences, 17, 3669–3684, <https://doi.org/10.5194/bg-17-3669-2020>, 2020.

- Gasol, J. M., and del Giorgio, P. A.: Using flow cytometry for counting natural planktonic bacteria and understanding the structure of planktonic bacterial communities, *Scientia Marina*, 64, 197–224, 2000.
- 870 Gazeau, F., Van Wambeke, F., Marañón, E., Pérez-Lorenzo, M., Alliouane, S., Stolpe, C., Blasco, T., Leblond, N., Zäncker B., Engel A., Marie, B., Dinasquet, J., and Guieu C.: Impact of dust addition on the metabolism of Mediterranean plankton communities and carbon export under present and future conditions of pH and temperature, *Biogeosciences*, in press, 2021.
- 875 Godwin, C. M., and Cotner, J. B.: Aquatic heterotrophic bacteria have highly flexible phosphorus content and biomass stoichiometry, the *ISME Journal*, 9, 2324–2327, doi:10.1038/ismej.2015.34, 2015.
- Guieu, C., and Ridame, C.: Impact of atmospheric deposition on marine chemistry and biogeochemistry, in: *Atmospheric Chemistry in the Mediterranean Region*, volume 2 –
880 From Air pollutants Sources to Impacts, Dulac, F., Sauvage, S., Hanoumou, E., Eds Springer, Switzerland, IBSN 978-3-030-82385-6, Chapter 22, in press.
- Guieu, C., Dulac, F., Desboeufs, K., Wagener, T., Pulido-Villena, E., Grisoni, J.-M., Louis, J., Ridame, C., Blain, S., Brunet, C., Bon Nguyen, E., Tran, S., Labiadh, M., and Dominici, J.-M.: Large clean mesocosms and simulated dust deposition: a new methodology to
885 investigate responses of marine oligotrophic ecosystems to atmospheric inputs, *Biogeosciences*, 7, 2765–2784, doi: 10.5194/BG-7-2765-2010, 2010.
- Guieu, C., Aumont, O., Paytan, A., Bopp, L., Law, C. S., Mahowald, N., Achterberg, E. P., Marañón, E., Salihoglu, B., Crise, A., Wagener, T., Herut, B., Desboeufs, K., Kanakidou, M., Olgun, N., Peters, F., Pulido-Villena, E., Tovar-Sanchez, A., and
890 Völker, C.: The significance of episodicity in atmospheric deposition to Low Nutrient Low Chlorophyll regions, *Global Biogeochem. Cycles*, 28, 1179–1198, doi:10.1002/2014GB004852, 2014a.
- Guieu, C., Ridame, C., Pulido-Villena, E., Bressac, M., Desboeufs, K., and Dulac, F.: Impact of dust deposition on carbon budget: a tentative assessment from a mesocosm approach,
895 *Biogeosciences*, 11, 5621–5635, doi: 10.5194/bg-11-5621-2014, 2014b.

- 900 Guieu, C., D'Ortenzio, F., Dulac, F., Taillandier, V., Doglioli, A., Petrenko, A., Barrillon, S., Mallet, M., Nabat, P., and Desboeufs, K.: Process studies at the air-sea interface after atmospheric deposition in the Mediterranean Sea: objectives and strategy of the PEACETIME oceanographic campaign (May–June 2017), *Biogeosciences*, 17, 1–23, 2020, doi: 10.5194/bg-17-1-2020.
- Heimbürger, A., Losno, R., Triquet, S., Dulac F., and Mahowald, N. M.: Direct measurements of atmospheric iron, cobalt and aluminium-derived dust deposition at Kerguelen Islands, *Global Biogeochem. Cy.*, 26, GB4016, doi:10.1029/2012GB004301, 2012.
- 905 Hersbach, H., Bell, B., Berrisford, P., Biavati, G., Horányi, A., Muñoz Sabater, J., Nicolas, J., Peubey, C., Radu, R., Rozum, I., Schepers, D., Simmons, A., Soci, C., Dee, D., Thépaut, J-N.: ERA5 hourly data on single levels from 1979 to present. Copernicus Climate Change Service (C3S) Climate Data Store (CDS). doi: 10.24381/cds.adbb2d47, 2018.
- 910 Herut, B., Zohary, T., Krom, M. D., Mantoura, R. F. C., Pitta, P., Psarra, S., Rassoulzadegan, F., Tanaka, T. and Thingstad, T. F.: Response of East Mediterranean surface water to Saharan dust: On-board microcosm experiment and field observations, *Deep-Sea Research II* 52 (2005) 3024–3040, 2005.
- 915 Herut, B., Rahav, E., Tsagaraki, T. M., Giannakourou, A., Tsiola, A., Psarra, S., Lagaria, A., Papageorgiou, N., Mihalopoulos, N., Theodosi, C. N., Violaki, K., Stathopoulou, E., Scoullou, M., Krom, M. D., Stockdale, A., Shi, Z., Berman-Frank, I., Meador, T. B., Tanaka, T., and Paraskevi, P.: The potential impact of Saharan dust and polluted aerosols on microbial populations in the East Mediterranean Sea, an overview of a mesocosm experimental approach, *Front. Mar. Sci*, 3, 226, doi: 10.3389/fmars.2016.00226, 2016.
- 920 Hoppe, H.-G., Ducklow, H., and Karrasch, B.: Evidence for dependency of bacterial growth on enzymatic hydrolysis of particulate organic matter in the mesopelagic ocean, *Mar. Ecol. Prog. Ser.*, 93, 277–283, 1993.
- 925 Ibello, V., Cantoni, C., Cozzi, S., and Civitarese, G.: First basin-wide experimental results on N₂ fixation in the open Mediterranean Sea, *Geophys. Res. Lett.*, 37, L03608, doi:10.1029/2009GL041635, 2010.

- Izquierdo, R., Benítez-Nelson, C. R., Masqué, P., Castillo, S., Alastuey, A., and Àvila, A.: Atmospheric phosphorus deposition in a near-coastal rural site in the NE Iberian Peninsula and its role in marine productivity, *Atmos. Environ.*, 49, 361–370, doi: 10.1016/j.atmosenv.2011.11.007, 2012.
- 930 Jumars, P. A., Penry, D. L., Baross, J. A., Perry, M. A., and Frost, B. W.: Closing the microbial loop : dissolved carbon pathway to heterotrophic bacteria from incomplete ingestion, digestion and absorption in animals, *Deep-Sea Research*, 483–495, 1989.
- Kamykowski, D., and Zentara, S. J.: Nitrate and silicic acid in the world ocean: Patterns and processes, *Mar. Ecol. Prog. Ser.*, 26, 47–59, 1985.
- 935 Kanakidou, M., Myriokefalitakis, S., and Tsigaridis, K.: Aerosols in atmospheric chemistry and biogeochemical cycles of nutrients, *Environ. Res. Lett.*, 13, 063004, doi: 10.1088/1748-9326/aabcbd, 2018.
- Kanakidou, M., Myriokefalitakis, S., and Tsagkaraki, M.: Atmospheric inputs of nutrients to the Mediterranean Sea, *Deep Sea Research Part II: Topical Studies in Oceanography*, 940 171, 104606, doi: 10.1016/j.dsr2.2019.06.014, 2020.
- Kirchman, D. L.: Leucine incorporation as a measure of biomass production by heterotrophic bacteria, in: *Handbook of methods in aquatic microbial ecology*, edited by : Kemp, P.F., Sherr, B.F., Sherr, E.B., and Cole, J.J., Lewis, Boca Raton, 509-512, 1993.
- Kouvarakis, G., Mihalopoulos, N., Tselepides, T., and Stavrakakis, S.: On the importance of 945 atmospheric nitrogen inputs on the productivity of eastern Mediterranean, *Global Biogeochemical Cycles*, 15, 805–818, doi:10.1029/2001GB001399, 2001.
- Krom, M. D., Herut, B., and Mantoura, R. F. C.: Nutrient budget for the eastern Mediterranean: Implication for phosphorus limitation, *Limnol. Oceanogr*, 49, 1582–1592, doi: 10.4319/lo.2004.49.5.1582, 2004.
- 950 Louis, J., Bressac, M., Pedrotti, M.-L., and Guieu, C.: Dissolved inorganic nitrogen and phosphorus dynamics in sea water following an artificial Saharan dust deposition event, *Frontiers Marine Sci.*, 2, article 27, doi: 10.3389/fmars.2015.00027, 2015.
- Løvdal, T., Skjoldal, E. F., Heldal, M., Norland, S., and Thingstad, T. F.: Changes in Morphology and Elemental Composition of *Vibrio splendidus* Along a Gradient from

- 955 Carbon-limited to Phosphate-limited Growth, *Microb. Ecol.*, 55, 152–161, doi:
10.1007/s00248-007-9262-x, 2008.
- Makino, W., Cotner, J. B., Sterner, R. W., and Elser, J. J.: Are bacteria more like plants or
animals? Growth rate and resource dependence of bacterial C : N : P stoichiometry,
Functional Ecology, 17, 121–130, 2003.
- 960 Malits, A., Cattaneo, R., Sintes, E., Gasol, J. M., Herndl, G. J., and Weinbauer, M.: Potential
impacts of black carbon on the marine microbial community, *Aquat Microb Ecol.*, 75,
27–42, doi: 10.3354/ame01742, 2015.
- Marañón, E., Fernández, A., Mouriño-Carballido, B., Martínez-García, S., Teira, E.,
Cermeño, P., Chouciño, P., Huete-Ortega, M., Fernández, E., Calvo-Díaz, A., Morán,
965 X. A. G., Bode, A., Moreno-Ostos, E., Varela, M. M., Patey, M. D., and Achterberg, E.
P.: Degree of oligotrophy controls the response of microbial plankton to Saharan dust,
Limnology and Oceanography, 55, 2339–2352, 2010.
- Marañón, E., Van Wambeke, F., Uitz, J., Boss, E. S., Dimier, C., Dinasquet, J., Angel, A.,
Haëntjens, N., Pérez-Lorenzo, M., Taillandier, V., and Zäncker, B.: Deep maxima of
970 phytoplankton biomass, primary production and bacterial production in the
Mediterranean Sea, *Biogeosciences*, 18, 1749–1767, doi:10.5194/bg-18-1749-2021,
2021.
- Mari, X., Guinot, B., Chu, V. T., Brune, J., Lefebvre, J.-P., Pradeep Ram, A. S., Raimbault,
P., Dittmar, T., and Niggemann, J.: Biogeochemical Impacts of a Black Carbon Wet
975 Deposition Event in Halong Bay, Vietnam, *Front. Mar. Sci*, 6, article 185, doi:
10.3389/fmars.2019.00185, 2019.
- Marie, D., Simon, N., Guillou, L., Partensky, F., and Vaultot, D.: Flow Cytometry Analysis of
Marine Picoplankton, in: *In Living Color: Protocols in Flow Cytometry and Cell
Sorting*, edited by: Diamond, R. A., and Demaggio, S., Springer, Berlin, Heidelberg,
980 421–454, 2000.
- Markaki, Z., Loye-Pilot, M. D., Violaki, K., Benyahya, L., and Mihalopoulos, N.: Variability
of atmospheric deposition of dissolved nitrogen and phosphorus in the Mediterranean
and possible link to the anomalous seawater N/P ratio, *Marine Chemistry*, 120, 187–
194, doi: 10.1016/j.marchem.2008.10.005, 2010.

- 985 Martiny, A. C., Pham, C. T. A., Primeau, F. W., Vrugt, J. A., Moore, J. K., Levin, S. A., and Lomas, M. W.: Strong latitudinal patterns in the elemental ratios of marine plankton and organic matter, *Nature geosciences*, 6, 279–283, doi: 10.1038/ngeo1757, 2013.
- Mermex Group.: Marine ecosystems' responses to climatic and anthropogenic forcings in the Mediterranean, *Progress in Oceanography*, 91, 97–166, doi: 10.1016/j.pocean.2011.02.003, 2011.
- 990
- Mescioglou E., Rahav E., Frada M.J., Rosenfeld S., Raveh O., Galletti Y., Santinelli C., Herut B., Paytan A.: Dust-associated airborne microbes affect primary and bacterial production rates, and eukaryote diversity, in the Northern Red Sea: A mesocosm approach. *Atmosphere*, 10, article 358, doi: 10.3390/atmos10070358, 2019.
- 995 Moreno, A. R., and Martiny, A. C.: Ecological stoichiometry of ocean plankton, *Ann. Rev. Mar. Sci.*, 10, 43–69, 2018.
- Nagata, T.: Carbon and Nitrogen content of natural planktonic bacteria, *Appl. Environ. Microbiol.*, 52, 28–32, 1986.
- Orsini, D., Ma, Y., Sullivan, A., Sierau, B., Baumann, K., and Weber, R.: Refinements to the Particle-Into-Liquid Sampler (PILS) for Ground and Airborne Measurements of Water Soluble Aerosol Composition, *Atmospheric Environment*, 37, 1243–1259, 2003.
- 1000
- Omand, M. M. and Mahadevan, A.: The shape of the oceanic nitracline, *Biogeosciences*, 12, 3273–3287, doi: 10.5194/bg-12-3273-2015, 2015.
- Pradeep Ram, A. S., and Sime-Ngando, T.: Resources drive trade-off between viral lifestyles in the plankton: evidence from freshwater microbial microcosms, *Environ Microbiol*, 12, 467–479, doi: 10.1111/j.1462-2920.2009.02088.x, 2010.
- 1005
- Prieur, L., D'Ortenzio, F., Taillandier, V. and Testor, P.: Physical oceanography of the Ligurian sea. In: Migon C., Sciandra A. & Nival P. (eds.), *the Mediterranean sea in the era of global change (volume 1), evidence from 30 years of multidisciplinary study of the Ligurian sea*, ISTE Sci. Publ. LTD, 49–78. doi:10.1002/9781119706960.ch3, 2020.
- 1010

- Pujo-Pay, M., and Raimbault, P.: Improvements of the wet-oxidation procedure for simultaneous determination of particulate organic nitrogen and phosphorus collected on filters, *Mar. Ecol. Prog. Ser.*, 105, 203–207, 1994.
- 1015 Pulido-Villena, E., Wagener, T., and Guieu, C.: Bacterial response to dust pulses in the western Mediterranean: Implications for carbon cycling in the oligotrophic ocean, *Global Biogeochem. Cycles*, 22, GB1020, doi:10.1029/2007GB003091, 2008.
- Pulido-Villena, E., Rérolle, V., and Guieu, C.: Transient fertilizing effect of dust in P-deficient surface LNLC ocean. *Geophysical Research Letters*, 37, L01603, doi:10.1029/2009GL041415, 2010.
- 1020
- Pulido-Villena, E., Baudoux, A.-C., Obernosterer, I., Landa, M., Caparros, J., Catala, P., Georges, C., Harmand, J., and Guieu, C.: Microbial food web dynamics in response to a Saharan dust event: results from a mesocosm study in the oligotrophic Mediterranean Sea, *Biogeosciences*, 11, 337–371, 2014.
- 1025 Pulido-Villena, E., Desboeufs, K., Djaoudi, K., Van Wambeke, F., Barrillon, S., Doglioli, A., Petrenko, A., Taillandier, V., Fu, F., Gaillard, T., Guasco, S., Nunige, S., Triquet, S., and Guieu, C.: Phosphorus cycling in the upper waters of the Mediterranean Sea (Peacetime cruise): relative contribution of external and internal sources, *Biogeosciences Discuss.*, [preprint], <https://doi.org/10.5194/bg-2021-94>, in review, 2021.
- 1030
- Rahav, E., Herut, B., Levi, A., Mulholland, M. R., and Berman-Frank, I.: Springtime contribution of dinitrogen fixation to primary production across the Mediterranean Sea. *Ocean Sci.* 9, 489–498. doi: 10.5194/os-9-489-2013, 2013a
- Rahav, E., Herut, B., Stambler, N., Bar-Zeev, E., Mulholland, M. R., and Berman-Frank, I.: Uncoupling between dinitrogen fixation and primary productivity in the eastern Mediterranean Sea, *J. Geophys. Res. Biogeosci.*, 118, 195–202, doi:10.1002/jgrg.20023, 2013b.
- 1035
- Rahav, E., Paytan, A., Chien, C.-T., Ovadia, G., Katz, T., and Herut, B.: The Impact of Atmospheric Dry Deposition Associated Microbes on the Southeastern Mediterranean Sea Surface Water following an Intense Dust Storm, *Front. Mar. Sci.* 3, 127, doi: 10.3389/fmars.2016.00127, 2016.
- 1040

- Richon, C., Dutay, J. C., Dulac, F., Wang, R., Balkanski, Y., Nabat, P., Aumont, O.,
Desboeufs, K., Laurent, B., Guieu, C., Raimbault, P., and Beuvier, J.: Modeling the
impacts of atmospheric deposition of nitrogen and desert dust-derived phosphorus on
1045 nutrients and biological budgets of the Mediterranean Sea, *Prog. Oceanogr.*, 163, 21–
39, doi: 10.1016/j.pocean.2017.04.009, 2018.
- Ridame, C., Moutin, T., and C. Guieu.: Does phosphate adsorption onto Saharan dust explain
the unusual N/P ratio in the Mediterranean Sea? *Oceanologica Acta*, 26, 629–634, doi:
10.1016/S0399-1784(03)00061-6, 2003.
- 1050 Ridame, C., Le Moal, M., Guieu, C. Ternon, E., Biegala, I., L'Helguen, S., and Pujo-Pay, M.:
Nutrient control of N₂ fixation in the oligotrophic Mediterranean Sea and the impact
of Saharan dust events, *Biogeosciences*, 8, 2773–2783, doi:10.5194/bg-8-2773-2011,
2011.
- Sala, M. M., Peters, F., Gasol, J. M., Pedros-Alio, C., Marrasse, C., and Vaque, D.: Seasonal
1055 and spatial variations in the nutrient limitation of bacterioplankton growth in the
northwestern Mediterranean, *Aquat. Microb. Ecol.*, 27, 47–56, 2002.
- Sandroni, V., Raimbault, P., Migon, C., Garcia, N., and Gouze, E.: Dry atmospheric
deposition and diazotrophy as sources of new nitrogen to northwestern Mediterranean
oligotrophic surface waters, *Deep-Sea Res. I*, 54, 1859–1870,
1060 doi:10.1016/j.dsr.2007.08.004, 2007.
- Taillandier, V., Prieur, L., D'Ortenzio, F., Ribera d'Alcala, M., and Pulido-Villena, E.:
Profiling float observation of thermohaline staircases in the western Mediterranean Sea
and impact on nutrient fluxes, *Biogeosciences*, 17, 3343–3366, 2020.
- Talarmin A, Van Wambeke F., Lebaron P., and Moutin T.: Vertical partitioning of phosphate
1065 uptake among picoplankton groups in the low Pi Mediterranean Sea, *Biogeosciences*,
12: 1237–1247 doi:10.5194/bg-12-1237-2015, 2015.
- Tanaka, T., Thingstad, T. F., Christaki, U., Colombet, J., Cornet-Barthaux, V., Courties, C.,
Grattepanche, J.-D., Lagaria, A., Nedoma, J., Oriol, L., Psarra, S., Pujo-Pay, M., and
Van Wambeke, F.: Lack of P-limitation of phytoplankton and heterotrophic prokaryotes
1070 in surface waters of three anticyclonic eddies in the stratified Mediterranean Sea,
Biogeosciences, 8, 525–538, doi: 10.5194/bg-8-525-2011, 2011.

- 1075 Tovar-Sánchez, A., Rodríguez-Romero, A., Engel, A., Zäncker, B., Fu, F., Marañón, E.,
Pérez-Lorenzo, M., Bressac, M., Wagener, T., Triquet, S., Siour, G., Desboeufs, K., and
Guieu, C.: Characterizing the surface microlayer in the Mediterranean Sea: trace metal
concentrations and microbial plankton abundance, *Biogeosciences*, 17, 2349–2364,
<https://doi.org/10.5194/bg-17-2349-2020>, 2020.
- 1080 Thingstad, T., Krom, M. D., Mantoura, F., Flaten, G., Groom, S., Herut, B., Kress, N., Law,
C. S., Pasternak, A., Pitta, P., Psarra, S., Rassoulzadegan, F., Tanaka, T., Tselepides,
A., Wassmann, P., Woodward, M., Riser, C., Zodiatis, G., and Zohary, T.: Nature of
phosphorus limitation in the ultraoligotrophic eastern Mediterranean, *Science*, 309,
1068–1071, doi: 10.1126/science.1112632, 2005.
- 1085 Van Wambeke, F., Christaki, U., Giannakourou, A., Moutin, T., and Souvemerzoglou, K.:
Longitudinal and vertical trends of bacterial limitation by phosphorus and carbon in
the Mediterranean Sea, *Microb. Ecol.*, 43, 119–133, doi: 10.1007/s00248-001-0038-4,
2002.
- Van Wambeke, F., Gimenez, A., Duhamel, S., Dupouy, C., Lefevre, D., Pujo-Pay, M., and
Moutin, T.: Dynamics and controls of heterotrophic prokaryotic production in the
western tropical South Pacific Ocean: links with diazotrophic and photosynthetic
activity, *Biogeosciences*, 15: 2669–2689, doi: 10.5194/bg-15-2669-2018, 2018.
- 1090 Van Wambeke, F., Pulido-Villena, E., Catala, P., Dinasquet, J., Djaoudi, K., Engel, A., Garel,
M., Guasco, S., Marie, B., Nunige, S., Taillandier, V., Zäncker, B., and Tamburini, C.:
Spatial patterns of ectoenzymatic kinetics in relation to biogeochemical properties in
the Mediterranean Sea and the concentration of the fluorogenic substrate used,
Biogeosciences, 18, 2301–2323, doi:10.5194/bg-18-2301-2021, 2021.
- 1095 Yelton, A. P., Acinas, S. G., Sunagawa, S., Bork, P., Pedros-Alio, C., Chisholm, S. W.:
Global genetic capacity for mixotrophy in marine picocyanobacteria, *ISME J* 10:2946-
2957, 2016.
- 1100 Zhang, J.-Z., and Chi, J.: Automated analysis of nano-molar concentrations of phosphate in
natural waters with liquid waveguide, *Environ. Sci. Technol.*, 36, 1048–1053, doi :
10.1021/es011094v, 2002.

Table 1. Main biogeochemical features/trophic conditions during the PEACETIME cruise. For TYR, ION and FAST sites investigated over several days, means \pm sd are indicated. ITChla: Integrated total chlorophyll a (Chla + dvChla). IPP: Integrated particulate primary production; IBP: integrated heterotrophic prokaryotic production. Integrations from surface to 200 m depth for all data expect IPP, integrated down to the depth of 1% Photosynthetically Active Radiation (PAR) level.

	sampling date	Lat. °N	Long. °E	Temp. at 5 m °C	Bottom depth m	DCM depth m	ITChl a mg chla m ⁻²	IPP mg C m ⁻² d ⁻¹	IBP mg C m ⁻² d ⁻¹
ST1	May 12	41°53.5	6°20	15.7	1580	49	35.0	284	51
ST2	May 13	40°30.36	6°43.78	17.0	2830	65	32.7	148	55
ST3	May 14	39°0.8.0	7°41.0	14.3	1404	83	23.2	140	77
ST4	May 15	37°59.0	7°58.6	19.0	2770	64	29.2	182	66
ST5	May 16	38°57.2	11°1.4	19.5	2366	77	30.5	148	51
TYR	May 17-20	39°20.4	12°35.56	19.6	3395	80 \pm 6	29 \pm 3	170 \pm 35	57 \pm 3
ST6	May 22	38°48.47	14°29.97	20.0	2275	80	18.7	142	62
ST7	May 24	36°39.5	18°09.3	20.6	3627	87	24.2	158	57
ION	May 25-28	35°29.1	19°47.77	20.6	3054	97 \pm 5	29 \pm 2	208 \pm 15	51 \pm 9
ST8	May 30	36°12.6	16°37.5	20.8	3314	94	31.6	206	71
ST9	June 2	38°08.1	5°50.5	21.2	2837	91	36.1	214	64
FAST	June 2-7 and 9	37°56.8	2°54.6	21.0	2775	79 \pm 8	34 \pm 8	211 \pm 57	92 \pm 11
ST10	June 8	37°27.58	1°34.0	21.6	2770	89	28.9	nd	96

1110 **Table 2.** N budget at the short stations within the surface mixed layer (ML). Integrated stocks
 (NO₃, $\mu\text{mol N m}^{-2}$) and fluxes (heterotrophic prokaryotic N demand (hprokN demand),
 phytoplankton N demand (phytoN demand), in situ leucine aminopeptidase hydrolysis fluxes
 (LAP), dry atmospheric deposition of NO₃ and NH₄ (all fluxes in $\mu\text{mol N m}^{-2} \text{d}^{-1}$). Values
 presented as mean \pm sd. SD was calculated using propagation of errors: For hprokN demand
 1115 triplicate measurements at each depth and a C/N ratio of 7.3 ± 1.6 ; for phytoN demand
 triplicate measurements of PP at each depth and a C/N ratio of 7 ± 1.4 ; for LAP the analytical
 TAA error and the Vm and Km errors; for N₂fix the coefficient of variation was 10% for
 volumetric fluxes $> 0.1 \text{ nmole N l}^{-1} \text{d}^{-1}$ and 20% for lower values. For dry deposition, sd is
 based on the variability of the NO₃ and NH₄ concentrations solubilized from aerosols during
 1120 the occupation of the station (see methods section 2.2.1). MLD: mixed layer depth. na: not
 available because under LWCC detection limits.

		stocks	biological fluxes				Dry deposition	
stations	MLD	NO ₃	phytoN demand	hprokN demand	LAP	N ₂ fixation	NO ₃	NH ₄
	m	$\mu\text{mol N m}^{-2}$	$\mu\text{mol N m}^{-2} \text{d}^{-1}$	$\mu\text{mol N m}^{-2} \text{d}^{-1}$	$\mu\text{mol N m}^{-2} \text{d}^{-1}$	$\mu\text{mol N m}^{-2} \text{d}^{-1}$	$\mu\text{mol N m}^{-2} \text{d}^{-1}$	$\mu\text{mol N m}^{-2} \text{d}^{-1}$
ST1	21	na	1468 \pm 325	184 \pm 40	121 \pm 28	14.6 \pm 1.5	18.6 \pm 1.4	1.5 \pm 0.3
ST2	21	na	481 \pm 161	163 \pm 35	48 \pm 24	10.7 \pm 1.1	23.7 \pm 2.2	4.1 \pm 0.9
ST3	11	na	282 \pm 82	126 \pm 28	40 \pm 17	7.8 \pm 0.8	33.8 \pm 3.6	4.7 \pm 0.5
ST4	15	na	246 \pm 80	132 \pm 28	83 \pm 20	10.7 \pm 1.1	23.8 \pm 2.9	6.3 \pm 2.6
ST5	9	261 \pm 22	112 \pm 29	42 \pm 9	17 \pm 12	4.8 \pm 0.5	27.0 \pm 7.5	7.9 \pm 1.8
ST6	18	162 \pm 14	410 \pm 116	204 \pm 44	48 \pm 24	9.1 \pm 0.9	15.0 \pm 0.6	9.3 \pm 0.7
ST7	18	162 \pm 14	226 \pm 123	148 \pm 33	83 \pm 18	10.5 \pm 1.1	23.6 \pm 1.9	8.0 \pm 1.2
ST8	14	911 \pm 77	274 \pm 66	130 \pm 33	25 \pm 8	4.3 \pm 0.5	13.4 \pm 1.7	3.8 \pm 0.6
ST9	7	819 \pm 70	259 \pm 70	85 \pm 22	21 \pm 6	3.4 \pm 0.4	27.4 \pm 3.8	13.5 \pm 0.8
ST10	19	2074 \pm 176	495 \pm 31	294 \pm 64	42 \pm 26	13.6 \pm 1.4	23.9 \pm 3.4	4.1 \pm 0.4

Table 3. Characteristics and nutrient fluxes estimated in the 2 rain samples collected during the PEACETIME cruise at ION and FAST.

event	Rain ION	Rain FAST
Date and local time	29/05 05:08-6:00	05/06 02:36-3:04
Estimated precipitation (mm)	3.5 ± 1.2	5.7 ± 1.4
DIP Flux nmol P m ⁻²	663 ± 227	1146 ± 290
DOP Flux nmol P m ⁻²	974 ± 334	908 ± 230
POP fluxes nmol P m ⁻²	239 ± 82	8801 ± 2227
NO3 Flux μmol N m ⁻²	67 ± 22	341 ± 86
NH4 Flux μmol N m ⁻²	71 ± 24	208 ± 53
DIN Flux μmol N m ⁻²	138 ± 47	550 ± 139

1130 **Figure legends**

Figure 1. Nitrate (NO₃) concentrations in the aerosols along the PEACETIME transect. The locations of two rain events are indicated by large black circles. Stations ST 1 to 4 were not sampled for nutrient analysis at a nanomolar level.

1135 **Figure 2.** Diagram showing the mixed layer (ML) and the bottom of the nitrate (NO₃) depleted layer (NDLb), delineated by the nitracline depth and the mixed layer depth (MLD) as defined in this study.

Figure 3. a) Evolution of the wind speed during the PEACETIME cruise. The stations are indicated in yellow and dates in black. Vertical dotted lines delineate the beginning and the end of the ship's deployment at TYR, ION and FAST. The two rain events collected on board are indicated by the solid vertical red arrows and surrounding observed rain events by horizontal dashed red arrows. b) Distribution of nitrate (NO₃) in the upper 100 m of the water column. The MLD (in red) and nitracline (in brown) are indicated.

1140

Figure 4. Average concentration of nitrate (NO₃) in the ML and NDLb, and NO₃ flux from the ML into the NDLb. The stations have been classified into 4 groups (1 in blue, 2 in green, 1145 3 in yellow, 4 in red, see section Results and Table S1 for definitions). Error bars indicate standard deviation around mean values for nitrate concentrations, and error propagation for the flux from ML to NDLb using a 0.5 m uncertainty in the MLD variation.

Figure 5. Evolution within the ML of heterotrophic prokaryotic production (BP), primary production (PP), heterotrophic prokaryotes (hprok) and *Synechococcus* (syn) abundances at 1150 FAST. The mixed layer depth is indicated by a red line.

Figure 6. Synthetic view of biogeochemical processes and exchanges between the ML and NDLb at FAST before the rain and evolution after the rain.

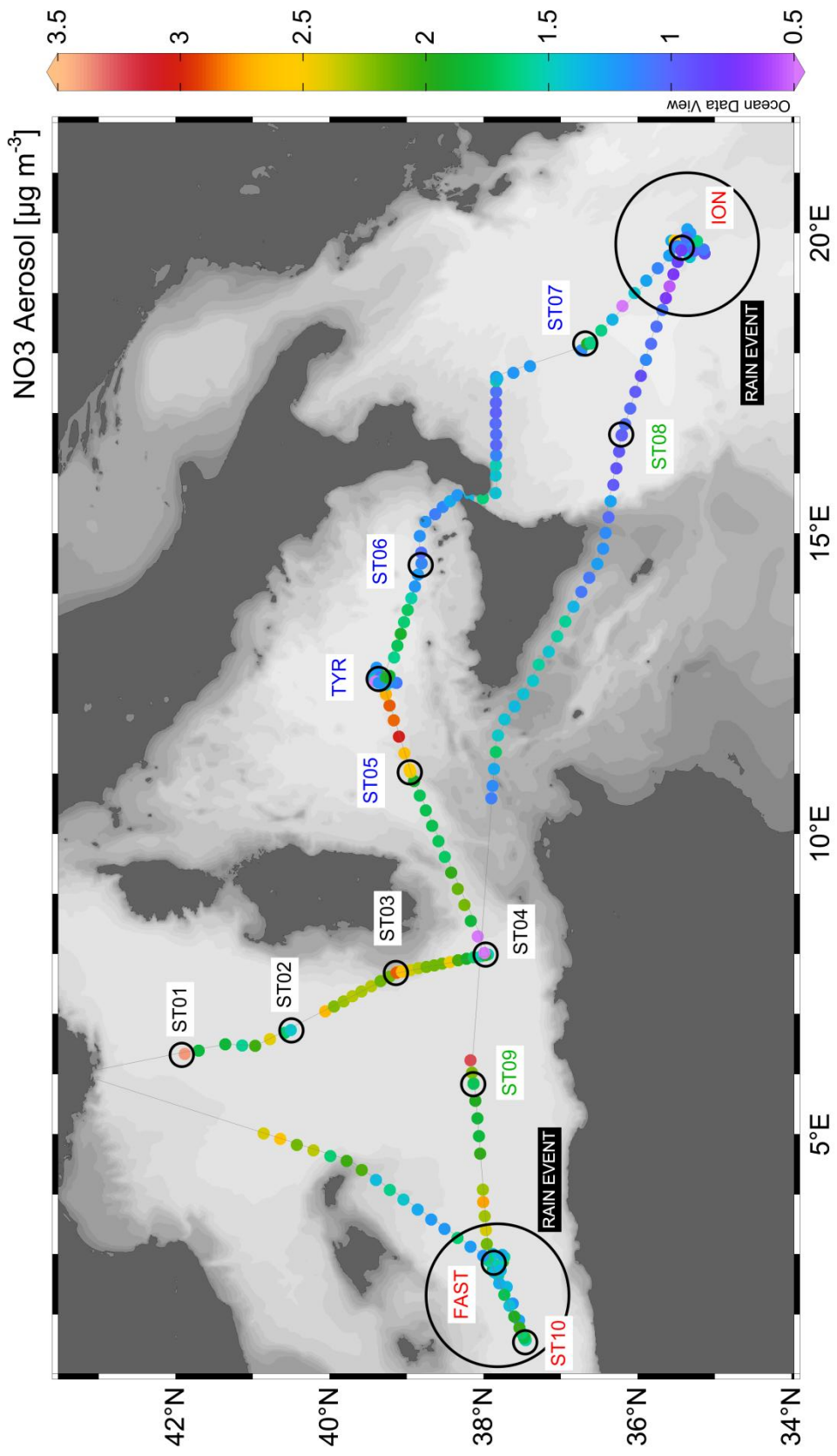


Fig. 1

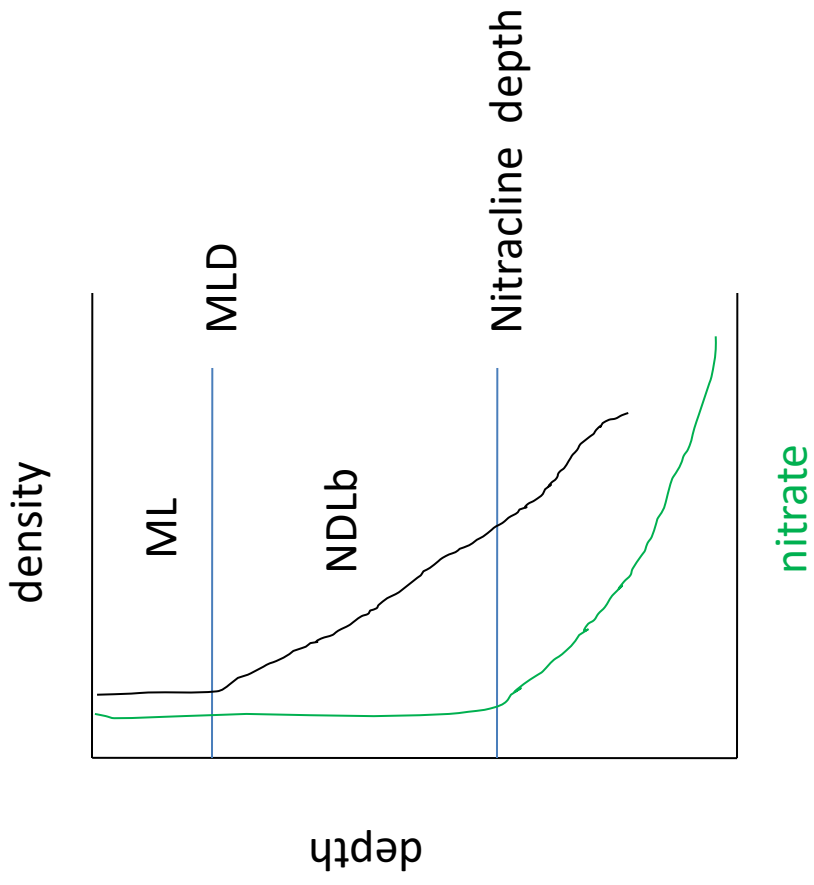


Fig. 2

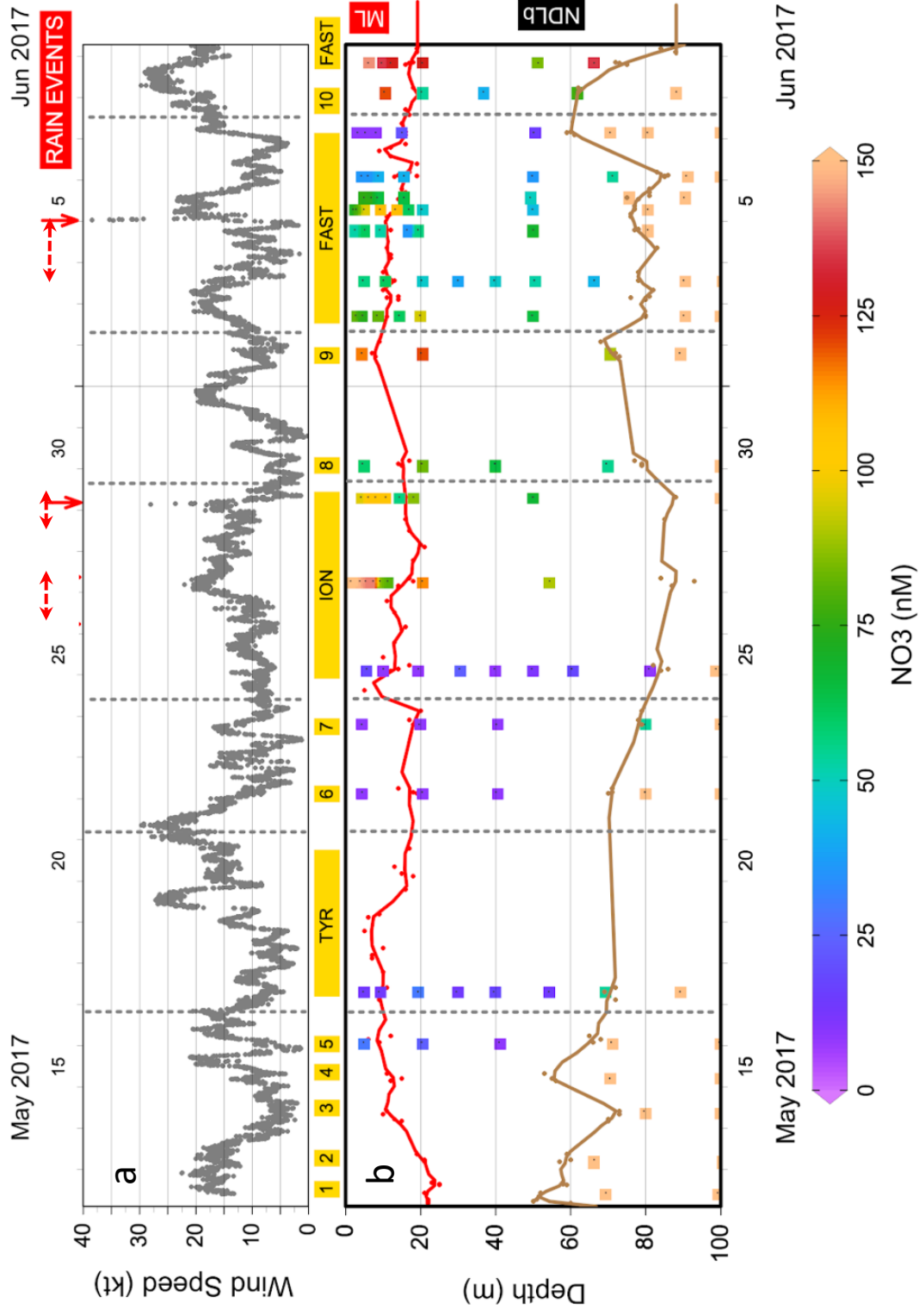


Fig. 3

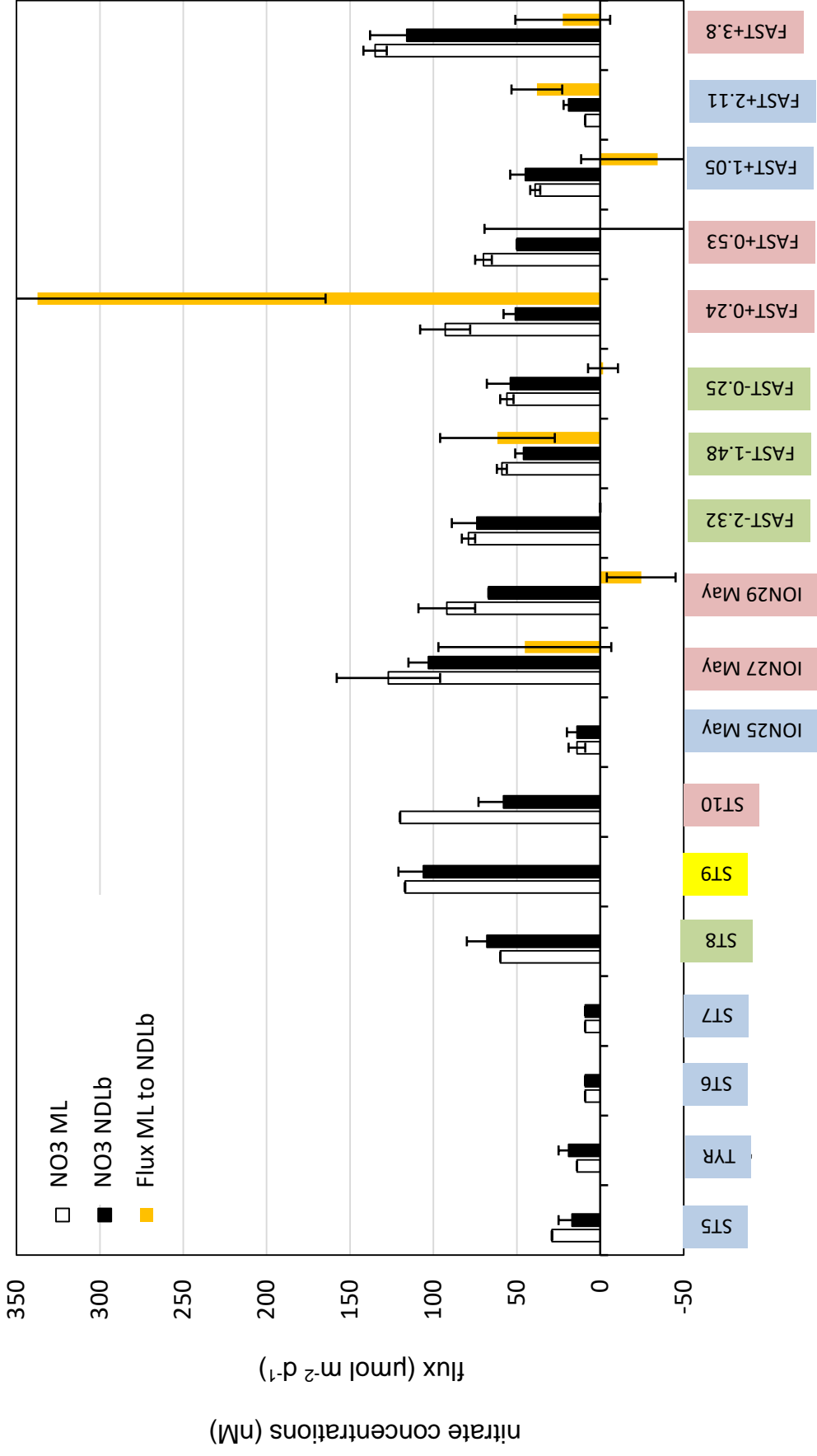


Fig. 4

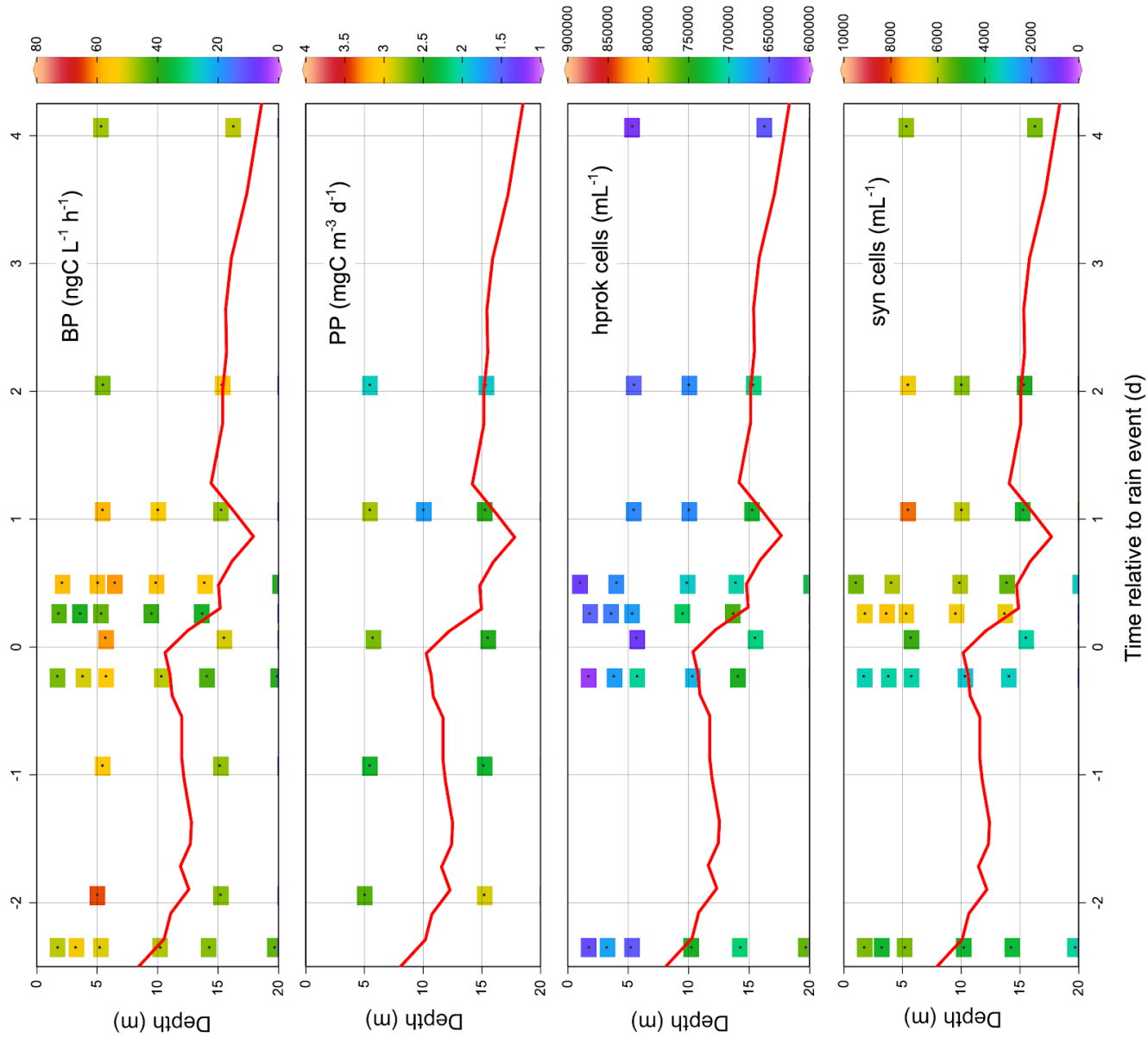


Fig. 5

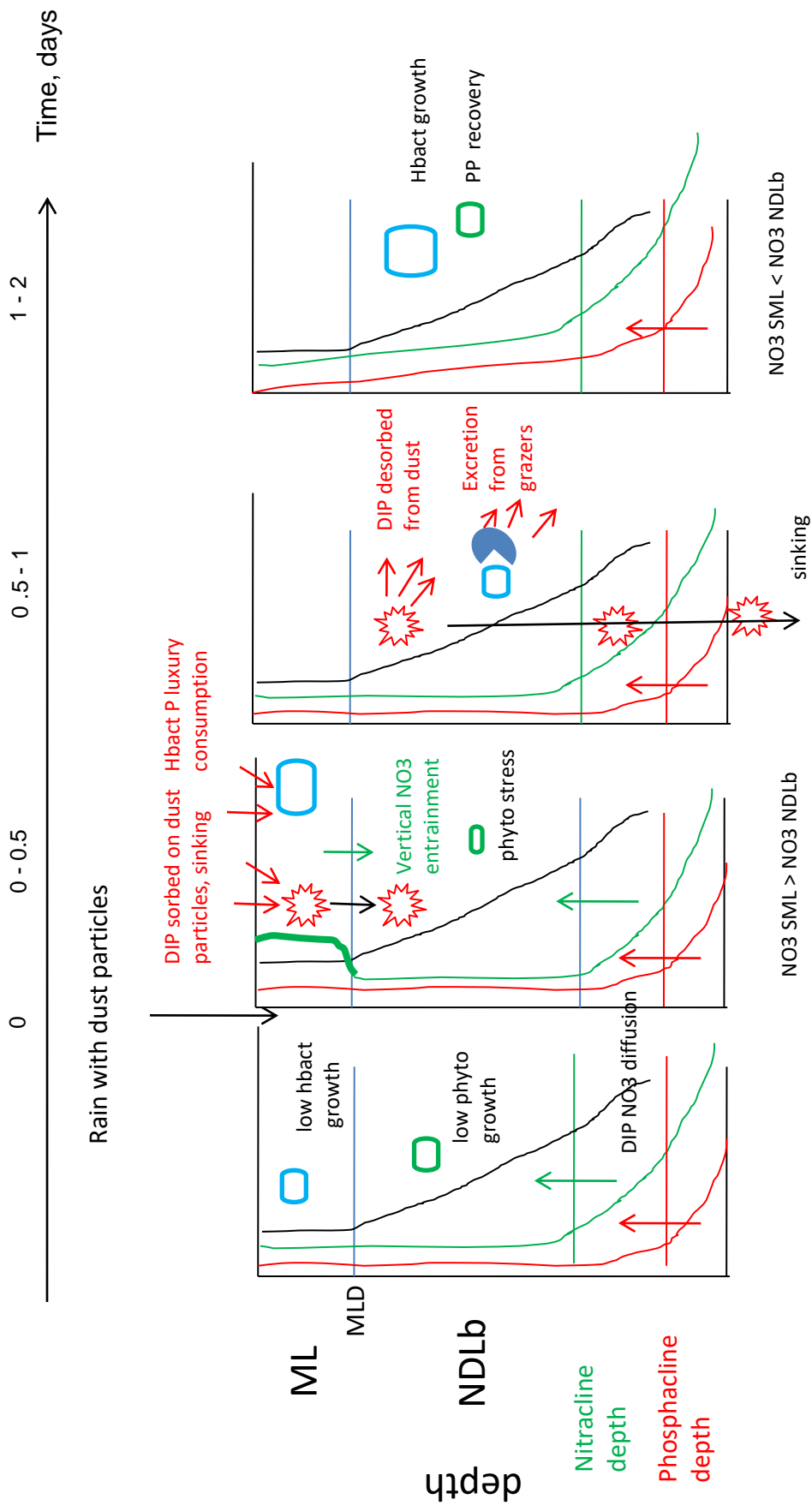


Fig. 6